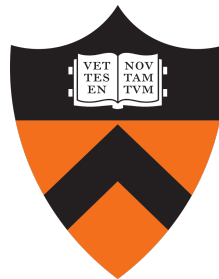


# Fractional Quantum Hall Phases in Bilayer Graphene

*Amir Shapour Mohammadi*

Junior Paper  
Department of Physics  
Princeton University  
Spring 2023



Adviser: Ali Yazdani  
Second reader: F. D. M. Haldane

This paper represents my own work in accordance with University regulations.

/s/ Amir Shapour Mohammadi

## **Abstract**

The purpose of this paper is to provide a self-contained review of fractional quantum Hall phases in bilayer graphene. An overview of the classical, integer, and fractional quantum Hall effects will be provided. We will focus on recent experimental techniques involving the use of scanning tunnelling spectroscopy to probe fractional quantum Hall phases in bilayer graphene. The central computation of this project will involve computing density of states of bilayer graphene using a tight-binding model and to compare with experimental results.

# Contents

<b>1</b>	<b>Introduction</b>	<b>1</b>
1.1	Classical planar electron . . . . .	1
1.2	Classical Hall effect . . . . .	2
1.3	Electromagnetism in quantum mechanics . . . . .	3
1.4	Planar electron in a magnetic field . . . . .	4
1.5	Landau levels . . . . .	4
1.6	Quantized Hall conductance . . . . .	6
<b>2</b>	<b>Fractional Quantum Hall Effect</b>	<b>8</b>
2.1	Interactions . . . . .	8
2.2	Laughlin states . . . . .	10
2.3	Plasma analogy . . . . .	11
2.4	Excitations . . . . .	12
2.5	Flux tubes . . . . .	13
2.6	Fractional statistics of Laughlin state . . . . .	14
2.7	Composite fermions . . . . .	15
2.8	Jain sequences . . . . .	16
2.9	Lambda levels . . . . .	17
2.10	Halperin bilayer state . . . . .	17
2.11	Moore-Read state . . . . .	18
<b>3</b>	<b>Bilayer Graphene</b>	<b>18</b>
3.1	Monolayer graphene . . . . .	19
3.1.1	Tight-binding model . . . . .	20
3.1.2	Magnetic field . . . . .	21
3.2	Bilayer graphene . . . . .	23
3.3	Scanning tunnelling spectroscopy . . . . .	25
3.4	Fractional quantum Hall effect in bilayer graphene . . . . .	29
<b>4</b>	<b>Conclusions</b>	<b>30</b>
<b>References</b>		<b>34</b>

# 1 Introduction

The discovery of quantum Hall effects in the 1980s has immensely changed the landscape of condensed matter physics. The (classical) Hall effect was discovered by Edwin Hall in 1879 and demonstrated the presence of a transverse so-called Hall resistivity  $\rho_H = \rho_{xy}$  when an electric field drives current through a 2-dimensional sample and a magnetic field is applied perpendicular to the plane. The explanation of this phenomena is purely classical. The quantum treatment of the problem significantly modifies the electron dynamics, with the introduction of quantized energy levels, known as Landau levels, which quench the kinetic energy. In 1980 using a high mobility silicon metal-oxide-semiconductor field-effect transistor (MOSFET), von Klitzing demonstrated that the Hall resistivity was quantized in units of the quantum resistivity  $R_K = h/e^2$ , and a relatively straightforward explanation was derived shortly after using the Landau level picture. The plateau of the Hall resistivity is complemented by the vanishing of the longitudinal resistivity  $\rho_{xx}$  in the bulk. Increments in the Hall resistivity were seen at integral filling factors  $\nu$ , or  $\nu$  completely filled Landau levels (as opposed to partially filled). In 1982, the fractional quantum Hall effect was discovered by Tsui and Stormer in which they found a relative dip in the longitudinal resistivity and a plateau of the Hall resistivity at fractional filling factor  $\nu = 1/3$ , corresponding to fractionally filling the lowest Landau level at 1/3. The explanation relies on electron interactions and was theorized by Laughlin in 1983 with his wave function ansatz at fractionally filling factors  $\nu = 1/m$  which was greatly supported by numerical simulations. With cleaner samples, fractional quantum Hall (FQH) phases were detected at many fractional filling factors  $\nu = p/q$  ( $q$  odd), including some even-denominator states. There are numerous novel phenomena associated with these FQH phases including fractional charge and anyonic statistics. Although it seems they have different origins, the IQH and FQH effects can be connected by considering bound states of electrons and an even number of magnetic flux quanta producing so-called composite fermions. We will discuss many of the interesting properties of these states. Many other fields have been born out of the quantum Hall effect including the topological insulator, fractional Chern insulator, quantum spin Hall effect, and quantum Hall ferromagnetism. We will explore the current developments of FQH effects in bilayer graphene, and the use of scanning tunneling spectroscopy to probe them.

## 1.1 Classical planar electron

We begin with a brief review of the classical picture of the electron confined to 2 dimensions and derive the classical Hall effect. The language and perspective we develop in this section will be crucial to understanding the quantum treatment in subsequent sections. For this classical treatment, we follow the derivation in [4].

Consider a planar electron with charge  $q = -e$  and a magnetic field  $\mathbf{B} = B\hat{\mathbf{z}}$  applied perpendicular to the plane. For the moment we do not include an electric field. The Lagrangian and Hamiltonian of this system can be derived

$$L = \frac{1}{2}m\mathbf{v}^2 - q\mathbf{A} \cdot \mathbf{v}, \quad H = \frac{1}{2m}(\mathbf{p} - q\mathbf{A}) \quad (1)$$

respectively where  $\mathbf{A}$  is the magnetic vector potential ( $\mathbf{B} = \nabla \times \mathbf{A}$ ). We solve the electron equations of motion to obtain the position and velocity

$$\mathbf{r}(t) = (X + \zeta(t), \quad Y + \eta(t), \quad 0), \quad \mathbf{v}(t) = \dot{\mathbf{r}}(t) = \omega_c(-\eta(t), \quad \zeta(t), \quad 0) \quad (2)$$

where  $X = \mathbf{R}_x$ ,  $Y = \mathbf{R}_y$  and  $\zeta = r_0 \cos(\omega_c t)$ ,  $\eta = r_0 \sin(\omega_c t)$ , and  $\mathbf{R}$  and  $r_0$  are initial conditions.

The cyclotron frequency is given by  $\omega_c = qB/m$  and describes the rate of precession of the electron about the center of the orbit  $\mathbf{R}$ . The angular momentum and kinetic energy can be solved for in the symmetric gauge  $\mathbf{A} = (-By/2, Bx/2, 0)$  to obtain

$$L_z = \frac{\partial L}{\partial \dot{\theta}} = (\mathbf{r} \times \mathbf{p})_z = \frac{1}{2}eB(R^2 - r_0^2), \quad T = \frac{1}{2}m\omega_c^2 r_0^2. \quad (3)$$

There are no surprises here. The electron undergoes cyclotron motion with frequency  $\omega_c$ .

## 1.2 Classical Hall effect

We now introduce an in-plane electric field  $\mathbf{E}$ . We describe the conductivity and resistivity as rank-2 tensors which obey Ohm's law

$$J_\mu = \sigma_{\mu\nu} E_\nu, \quad E_\mu = \rho_{\mu\nu} J_\nu, \quad \sigma_{\mu\nu} = (\rho^{-1})_{\mu\nu}. \quad (4)$$

Note that this is a slight generalization to the introductory treatment of these quantities as scalars, but this treatment is justified naturally. We assume rotational symmetry in our sample which gives us  $\sigma_{xx} = \sigma_{yy}$ ,  $\sigma_{xy} = -\sigma_{yx}$ . With this simplification we obtain

$$\rho_{xx} = \rho_{yy} = \frac{\sigma_{xx}}{\sigma_{xx}^2 + \sigma_{xy}^2}, \quad \rho_{xy} = -\rho_{yx} = \frac{-\sigma_{xy}}{\sigma_{xx}^2 + \sigma_{xy}^2}. \quad (5)$$

We will now describe the dynamics of the electron system. The Lorentz force can be written

$$m \frac{d^2 \mathbf{r}}{dt^2} = q(\mathbf{E} + \mathbf{v} \times \mathbf{B}) \quad (6)$$

where  $m$  is the mass of the electron. We assume fixed, time-independent electric and magnetic fields  $\mathbf{E} = E\hat{\mathbf{x}}$ ,  $\mathbf{B} = B\hat{\mathbf{z}}$  and solve for the velocity

$$\mathbf{v}(t) = (-r_0\omega_c \sin(\omega_c t), \quad r_0\omega_c \cos(\omega_c t) + v_0, \quad 0) \quad (7)$$

which describes cyclotron motion with constant drift velocity  $\mathbf{v}_0 = \mathbf{E} \times \mathbf{B}/B^2 = -E/B\hat{\mathbf{y}} = v_0\hat{\mathbf{y}}$ . As before,  $r_0$  is an initial condition. Neglecting the cyclotron motion, the electric current becomes

$$\mathbf{J}(t) = n_e q \mathbf{v}(t) = (0, \quad n_e q E / B, \quad 0) = \boldsymbol{\sigma} \cdot \mathbf{E} \quad (8)$$

from which we obtain the conductivity

$$\boldsymbol{\sigma} = \begin{pmatrix} 0 & \sigma_{xy} \\ -\sigma_{xy} & 0 \end{pmatrix}, \quad \sigma_{xy} = n_e q / B. \quad (9)$$

and the resistivity

$$\boldsymbol{\rho} = \boldsymbol{\sigma}^{-1} = \begin{pmatrix} 0 & -\rho_{xy} \\ \rho_{xy} & 0 \end{pmatrix}, \quad \rho_{xy} = B / (n_e q) \quad (10)$$

The Hall conductivity (and resistivity) take values from a continuous range therefore cannot describe the quantized values of the IQH phase.

We now cover the integer quantum Hall effect through a quantum treatment of the planar electron. A brief overview of electromagnetism in quantum mechanics will be provided along with Landau levels and the corresponding electron wave functions, and quantized Hall resistivity. We also explain

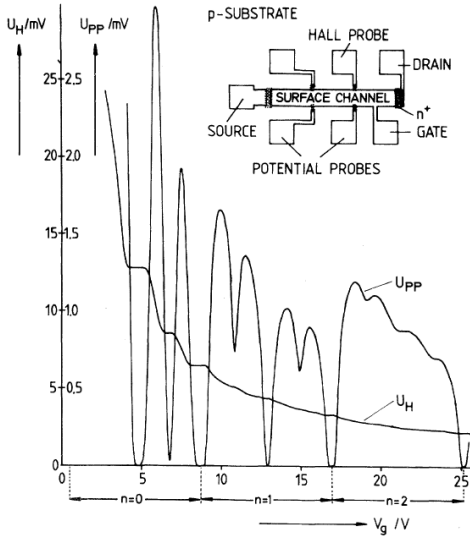


Figure 1: Quantized Hall resistivity and vanishing longitudinal resistivity as measured in von Klitzing’s seminal paper which was later interpreted as the integer quantum Hall effect [8].

the role of disorder in the size of the plateaus. Throughout this section, we (justifiably) do not include Coulomb interactions between the electrons. This inter-electron interaction will become crucial to the discussion of the fractional quantum Hall effect in the next section. We follow the derivations in [4].

### 1.3 Electromagnetism in quantum mechanics

Consider a particle of charge  $q$  and mass  $m$  in an electromagnetic field with vector potential  $\mathbf{A}$  and scalar potential  $\phi$ . The electromagnetic field couples to the particle through the minimal coupling

$$H = \frac{1}{2m}(\mathbf{p} - q\mathbf{A})^2 + q\phi \quad (11)$$

where  $\mathbf{p} = -i\hbar\nabla$  is the momentum operator and satisfies the commutation relation  $[x_\mu, p_\nu] = i\hbar\delta_{\mu\nu}$ . We naturally require that observables are left unchanged under any gauge transformation

$$\mathbf{A} \mapsto \mathbf{A} + \nabla\Lambda, \quad \phi \mapsto \phi - \frac{\partial\Lambda}{\partial t} \quad (12)$$

which transforms the Hamiltonian and wave function as

$$\psi \mapsto U\psi, \quad H \mapsto UHU^\dagger, \quad U = \exp(iq\Lambda/\hbar) \quad (13)$$

where  $U$  is a unitary operator. Observables also transform as  $A \mapsto UAU^\dagger$ . To see that observables are left invariant under gauge transformation, note that for any density matrix  $\rho$ , we have

$$\langle A \rangle = \text{tr}(\rho A) \mapsto \langle UAU^\dagger \rangle = \text{tr}\left((U\rho U^\dagger)UAU^\dagger\right) = \text{tr}\left(U\rho AU^\dagger\right) = \text{tr}(\rho A) = \langle A \rangle \quad (14)$$

where we used the cyclic property of trace. Therefore although the wave function may change as a result of a gauge transformation, any observable quantities such as position, velocity, and current,

must remain invariant. This is very natural since the gauge arises from a redundancy, and so gauge transformed quantities describe the same physical situation.

## 1.4 Planar electron in a magnetic field

We now return to the planar electron in a perpendicular magnetic field  $\mathbf{B} = B\hat{\mathbf{z}}$ . For the moment, we do not consider any electric field. The (quantum) Hamiltonian can be written

$$H = \frac{1}{2m}(\mathbf{p} - q\mathbf{A})^2 \quad (15)$$

where  $\mathbf{A}$  is the vector potential. We solve for the velocity using the Heisenberg equation of motion

$$\mathbf{v} = \dot{\mathbf{r}} = \frac{i}{\hbar}[H, \mathbf{r}] = \frac{1}{m}(\mathbf{p} - q\mathbf{A}). \quad (16)$$

We define the mechanical momentum

$$\Pi = m\mathbf{v} = \mathbf{p} - q\mathbf{A} \quad (17)$$

which is an analog of the momentum we are familiar with from classical mechanics. It includes both the particle's momentum as well as momentum in the electromagnetic field, the combination of which is conserved,  $\dot{\Pi} = 0$ . We can rewrite the Hamiltonian as  $H = \Pi^2/2m$ . The mechanical momentum obeys the commutation relations  $[\Pi_x, \Pi_y] = i\hbar eB = -i\hbar^2/l^2$  where we introduce the magnetic length  $l = \sqrt{\hbar/eB}$ .

Recall that in the absence of a magnetic field, the kinetic momentum  $\mathbf{p}$  is the generator of translations

$$e^{-i\delta \cdot \mathbf{p}/\hbar} |\mathbf{x}\rangle = |\mathbf{x} - \delta\rangle. \quad (18)$$

In the present case, the generator of translations becomes

$$\mathbf{K} = \Pi + e\mathbf{B} \times \mathbf{r} \quad (19)$$

but note that unlike the momentum  $\mathbf{p}$ , the components of the generator  $\mathbf{K}$  do not commute with each other  $[K_x, K_y] = i\hbar^2/l^2$ . Therefore the translation operators do not commute

$$\mathcal{T}(\mathbf{a})\mathcal{T}(\mathbf{b}) = \mathcal{T}(\mathbf{b})\mathcal{T}(\mathbf{a})e^{-i[\mathbf{a}, \mathbf{b}]_z/l^2}, \quad \mathcal{T}(\mathbf{x}) = e^{-i\mathbf{x} \cdot \mathbf{K}/\hbar}. \quad (20)$$

This non-commutativity is the origin of the Aharonov-Bohm effect which we will not cover in depth but will be crucial to our understanding of the statistics of quasielectrons in fractional quantum Hall phases.

## 1.5 Landau levels

We will now rewrite the Hamiltonian as a more familiar harmonic oscillator. Note that since  $[\Pi_x, \Pi_y] \propto 1$ , the Hamiltonian is algebraically equivalent to that of a harmonic oscillator. This motivates us to solve the problem in terms of ladder operators just as the harmonic oscillator is solved. We introduce the ladder operators

$$a = \frac{l}{\sqrt{2\hbar}}(\Pi_x + i\Pi_y), \quad a^\dagger = \frac{l}{\sqrt{2\hbar}}(\Pi_x - i\Pi_y), \quad [a, a^\dagger] = 1 \quad (21)$$

using which we can rewrite the Hamiltonian and obtain its energy levels

$$H = \hbar\omega_c \left( a^\dagger a + \frac{1}{2} \right), \quad \varepsilon_n = \hbar\omega_c \left( n + \frac{1}{2} \right), \quad n \in \mathbb{Z}_{\geq 0} \quad (22)$$

which are called Landau levels. The eigenstates can be written as  $|n\rangle = 1/\sqrt{n!}(a^\dagger)^n |0\rangle$ . In analogy with the result from the classical treatment, we define the guiding center coordinates

$$\mathbf{R} = (X, Y) = \mathbf{r} + \frac{l^2}{\hbar} \hat{\mathbf{r}} \times \boldsymbol{\Pi}, \quad \mathbf{r} = (x, y) \quad (23)$$

which satisfy the commutation relations  $[X, Y] = -il^2$ ,  $[\mathbf{R}, \boldsymbol{\Pi}] = \mathbf{0}$  so that  $[\mathbf{R}, H] = 0$ . The last relation implies that the Landau levels are degenerate with respect to the guiding center coordinates  $X, Y$ . We will now investigate this degeneracy. In the symmetric gauge  $\mathbf{A} = (-By/2, Bx/2, 0)$ , the angular momentum operator can be expressed as

$$L_z = -\frac{\hbar^2}{2l^2}(X^2 + Y^2) + \frac{l^2}{2\hbar}(\Pi_x^2 + \Pi_y^2) \quad (24)$$

which is analogous to the expression we obtained in the classical treatment. Since  $[L_z, H] = 0$ , we have that each Landau level is degenerate with respect to angular momentum. We now reveal this degeneracy explicitly. We define the angular momentum raising and lowering operators

$$b = \frac{1}{\sqrt{2}l}(X - iY), \quad b^\dagger = \frac{1}{\sqrt{2}l}(X + iY), \quad [b, b^\dagger] = 1 \quad (25)$$

which satisfy the commutation relations  $[a, b] = [a^\dagger, b^\dagger] = 0$ . We can also rewrite the angular momentum operator as  $L_z = \hbar(a^\dagger a - b^\dagger b)$ . The eigenstates of the Hamiltonian can be written

$$|n, m\rangle = \frac{1}{\sqrt{(nm)!}}(a^\dagger)^n(b^\dagger)^m |0\rangle, \quad \langle n, m | n', m' \rangle = \delta_{n,n'}\delta_{m,m'}, \quad \sum_{n,m} |n, m\rangle \langle n, m| = \mathbf{1}. \quad (26)$$

Note that the eigenstate  $|n, m\rangle$  has angular momentum  $\langle n, m | L_z | n, m \rangle = \hbar(n - m)$ . Therefore for a fixed landau level  $n$ , the states  $|n, m\rangle$  represent states of the same energy but with different angular momentum.

Now that we understand the energy levels of the Hamiltonian and the origin of their degeneracies, we solve for the eigenstate wave functions. We express the ladder operators in real space [3]

$$\begin{aligned} a &= -\frac{i}{\sqrt{2}} \left( z + \frac{\partial}{\partial \bar{z}} \right), & a^\dagger &= \frac{i}{\sqrt{2}} \left( \bar{z} + \frac{\partial}{\partial z} \right) \\ b &= \frac{1}{\sqrt{2}} \left( \bar{z} + \frac{\partial}{\partial z} \right), & b^\dagger &= \frac{1}{\sqrt{2}} \left( z + \frac{\partial}{\partial \bar{z}} \right) \end{aligned} \quad (27)$$

where we have defined the complex variable  $z = x + iy$  and its conjugate  $\bar{z} = x - iy$ . We can solve for the wave function in the  $n = 0$  Landau level, referred to as the lowest Landau level (LLL), with zero angular momentum by solving the differential equation  $a |0, 0\rangle = b |0, 0\rangle = 0$ . We obtain the  $|0, 0\rangle$  wave function

$$\psi_{00}(\mathbf{r}) = \langle \mathbf{r} | 0, 0 \rangle = \frac{1}{\sqrt{2\pi l}} e^{-|z|^2/4} \quad (28)$$

and can obtain higher level wave functions by applying the raising operators  $a^\dagger, b^\dagger$ . The LLL wave

function with angular momentum  $m$  can be expressed as

$$\psi_{0m}(\mathbf{r}) = \frac{1}{\sqrt{2\pi 2^m m! l}} z^m e^{-|z|^2/4} \quad (29)$$

which corresponds to an electron (approximately) localized on an annular region of minimum radius  $r_m = \sqrt{2ml}$ , maximum radius  $r_{m+1}$ , and area  $A = \pi(r_{m+1}^2 - r_m^2) = 2\pi l^2$ . Note that the area occupied by each electron in the LLL is constant, irrespective of angular momentum. We utilize this picture to quantify the degeneracy of each Landau level. Given a disk geometry of radius  $R$  (area  $S = \pi R^2$ ), we only consider electron states inside this area, or states such that  $(\sqrt{2ml})^2 = 2ml^2 < R^2$ . Since each electron occupies an area  $2\pi l^2$ , the total number of electrons in the LLL is precisely  $S/2\pi l^2$ . This result holds for higher Landau levels. Note that the magnetic flux that penetrates the area occupied by a single electron is a constant  $BA = B \cdot 2\pi l^2 = h/e = \Phi_0$  called the flux quantum. In other words, there is precisely one electron state per flux quantum per Landau level. Increasing the magnetic field increases the number of electron states by raising maximum angular momentum. Thus there are  $N_\Phi = \Phi/\Phi_0$  angular momentum states in the LLL where  $\Phi = BS$  is the total area of the sample. Although we derived this result in the symmetric gauge with a disk geometry, we can obtain the same result in the Landau gauge<sup>1</sup> with a rectangular geometry.

The wave function will be of central importance when we discuss the FQH effect. Note that since the Schrodinger equation is linear, we can take linear combinations of the LLL states  $\psi_{0m}$  to generate new eigenstates. Since  $\psi_{0m}$  contains the factor  $z^m$ , the wave function

$$\psi(\mathbf{r}) = f(z) e^{-|z|^2/4} \quad (30)$$

where  $f(z)$  is holomorphic (complex-differentiable), or an arbitrary polynomial in  $z$ , is also an eigenstate of the LLL. This holomorphic degree of freedom will be used to construct FQH states in a later section.

## 1.6 Quantized Hall conductance

We now introduce an in-plane electric field  $\mathbf{E} = E\hat{\mathbf{x}}$ , arriving at the same physical setup we considered in the classical Hall effect. We cannot use the symmetric gauge since angular momentum is no longer conserved, so we instead use the Landau gauge  $\mathbf{A} = (0, Bx, 0)$ . It is a simple exercise to show that this vector potential still generates the perpendicular magnetic field  $\mathbf{B} = \nabla \times \mathbf{A} = B\hat{\mathbf{z}}$ . We obtain the Hamiltonian

$$H = \frac{1}{2m}(p_x^2 + (p_y - qBx)^2) + qEx. \quad (31)$$

It is simple to see that  $[H, p_y] = 0$  and so we have the ansatz eigenstate

$$\varphi(\mathbf{r}) = e^{ik_y y} \psi(x) \quad (32)$$

and we have the simplified Schrodinger equation

$$\left( \frac{1}{2m}(p_x^2 + (\hbar k_y - qBx)^2) + qEx \right) \psi(x) = \varepsilon_x \psi(x) \quad (33)$$

---

<sup>1</sup>The Landau could also have been used to solve this problem, resulting in wave functions which are translationally invariant in one direction, but the physics is the same.

which can be reformulated to obtain

$$\left( \frac{1}{2m}p_x^2 + \frac{1}{2}m\omega_c^2(x - X)^2 \right) \psi(x) = \left( \varepsilon_x - qEX - \frac{1}{2}m(E/B)^2 \right) \psi(x), \quad X = k_y l^2 + \frac{qE}{m\omega_c^2}. \quad (34)$$

Note that this is simply the Hamiltonian of a harmonic oscillator centered at position  $X$  with wave function given by

$$\psi_n(x) = \frac{1}{\sqrt{2^n n! l \sqrt{\pi}}} \exp\left(-\frac{(x - X)^2}{2l^2}\right) H_n((x - X)/l) \quad (35)$$

where  $H_n$  are Hermite polynomials. The corresponding energy levels are

$$\varepsilon_{n,X} = \hbar\omega_c \left( n + \frac{1}{2} \right) + qEX + \frac{1}{2}mE/B. \quad (36)$$

The first term corresponds to Landau levels, the second term is due to the electric potential, and the third term is due to  $\mathbf{E} \times \mathbf{B}$  drift. We can now compute the expectation values of the velocity operators

$$\langle \psi | v_x | \psi \rangle = \langle \psi | \Pi_x / m | \psi \rangle = 0, \quad \langle \psi | v_y | \psi \rangle = \langle \psi | \Pi_y / m | \psi \rangle = -E/B. \quad (37)$$

The conductivity tensor can be computed

$$\boldsymbol{\sigma} = \begin{pmatrix} 0 & \sigma_{xy} \\ -\sigma_{xy} & 0 \end{pmatrix}, \quad \sigma_{xy} = n_e q / B. \quad (38)$$

where  $n_e$  is the electron density. This is exact the result we derived from the classical treatment. The crucial difference is that now the energy levels are quantized. Therefore if we focus our attention to only filled Landau levels, the electron density  $n_e$  is also quantized. Explicitly,  $n_e = n\Phi/\Phi_0 = nB/\Phi_0 = n/2\pi l^2$  where  $n$  is the highest (fully) filled Landau level.

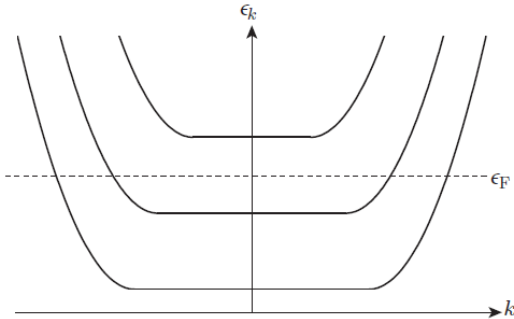


Figure 2: Landau level dispersion with confining potential near the edge of the sample [4].

We now provide a semiclassical derivation of the quantization of Hall conductivity using the edge state picture. There are quantum treatments of this problem, but they require formalism which for brevity we will not develop. The derivation provided here will suffice. We study the behavior along the edges of the sample. The sample has a confinement potential  $V(x, y) = V(y)$  which keeps the electrons on the sample. This confinement potential increases drastically near the edges and constitutes a large force  $\hat{\mathbf{y}}\partial\varepsilon/\partial y = \hat{\mathbf{y}}\partial V/\partial y$  on the electron which in the steady state is balanced by the magnetic Lorentz force  $q(\mathbf{v} \times \mathbf{B})_y = qv_x B$  from which we obtain the velocity  $v_x = (\partial\varepsilon/\partial y)/eB$ . We compute the edge current per Landau level. We only consider electrons above the chemical

potential as contributing to the edge current. These electrons are not localized to any atom. We denote the distance between the edge of the sample and the point where the energy band crosses the chemical potential as  $\Delta y$ . The current for a single edge per Landau level can be computed

$$I = J \cdot \Delta y = n_e q v \cdot \Delta y = \frac{qB}{h} \cdot q \cdot \frac{\partial \varepsilon / \partial y}{qB} \cdot \frac{q\Delta\mu}{\partial \varepsilon / \partial y} = \frac{e^2}{h} \Delta\mu \quad (39)$$

where  $n_e$  is the density of states per Landau level and  $q\Delta\mu = (\partial \varepsilon / \partial y)\Delta y$  is the difference in energy right at the edge of the sample (where the confinement potential is greatest) from the chemical potential. The Hall resistivity per Landau level becomes a constant

$$\rho_{xy} = \frac{\Delta\mu}{I} = \frac{h}{e^2} = R_K \quad (40)$$

where  $R_K = h/e^2$  has units of Ohms and is known as the von Klitzing constant. It is remarkable that the Hall resistivity is independent of all parameters of the system. Since current adds, the Hall resistivity for  $n$  fully occupied Landau levels is  $\rho_{xy} = R_K/n$ , or

$$\sigma_{xy} = \frac{-\rho_{xy}}{\rho_{xx}^2 + \rho_{xy}^2} = -\frac{1}{\rho_{xy}} = -\frac{n}{R_K} = -\frac{ne^2}{h} \quad (41)$$

where we used that  $\rho_{xx} = 0$ .

Although we have derived the quantization of the Hall resistivity, it is still not clear how the plateaus fit into the picture. To understand the plateaus, we have to consider the role of disorder in the system. The sample is not perfect as there are impurities that localize electrons in the bulk (irrelevant to cyclotron localization). As the filling factor is increased starting from  $\nu = 0$ , these localized states are filled first. Since the edge states have relatively high energy, they will not be filled until the localized bulk states have been filled. In the absence of disorder, all of the states in the bulk have the same energy, and so the chemical potential is precisely at the Landau level energy. However in the above argument, it was crucial that the Fermi energy intersected the confinement potential energy above the Landau level energy so that  $\Delta y$  is nonzero. Hence we see that disorder is the origin of the finite width of the Hall resistivity (or conductivity) plateau.

## 2 Fractional Quantum Hall Effect

We have discussed the integer quantum Hall effect and proved that it is a phenomena associated with fully filled Landau levels, or integer filling factors  $\nu$ . Soon after its discovery, the same experiment was conducted in cleaner, high-mobility GaAs-AlGaAs heterostructure at filling factor  $\nu < 1$ . Originally Tsui and Stormer attributed the fractional Hall conductivity and vanishing of longitudinal resistivity at  $\nu = 1/3$  as an effect of a Wigner crystal. However this explanation was not theoretically plausible, and a new explanation based on inter-electron interactions was sought. We will cover the role of interactions in the fractional quantum Hall effect, in particular Laughlin's ansatz for the wave function at filling factors  $\nu = 1/m$  ( $m$  odd), and the composite fermion picture.

### 2.1 Interactions

It is natural that inter-electron interactions play a significant role when the filling factor is fractional. There are unoccupied orbitals in the bulk for electrons to hop around, unlike the case of a fully filled Landau level where all orbitals in the bulk are occupied. A priori, it is not clear which

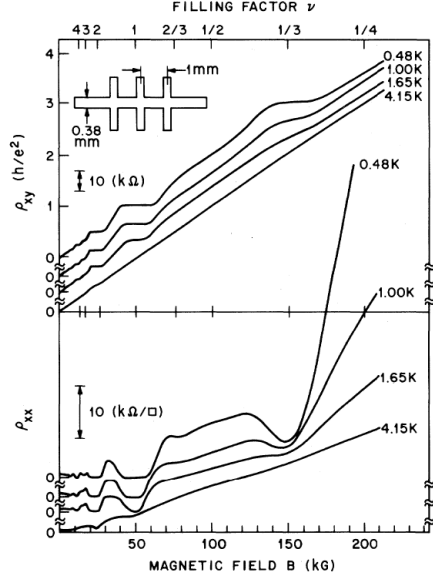


Figure 3: Hall plateau at fractional filling  $\nu = 1/3$  in Tsui's seminal paper which was later explained by Laughlin's ansatz wave function [14].

interaction could be responsible for the effects at fractional filling factor. When discussing the IQH effect, we did not consider spin (or we considered a spin-polarized system), and we did not consider inter-electron Coulomb interactions. We also did not consider spin-orbit coupling, but we will argue that it is negligible. We did include the exchange interaction in the integer filling factor case by requiring that multiple spin-polarized electrons cannot occupy the same orbital. We will now explore these interactions and show that the Coulomb interaction is crucial. We consider a system of  $N$  particles with the above interactions (without an electric field) [7]

$$H = \frac{1}{2m} \sum_{j=1}^N \mathbf{\Pi}_j^2 + \sum_{j=1}^N \sum_{k < j} \frac{e^2}{4\pi\epsilon_0 |\mathbf{x}_j - \mathbf{x}_k|} + g\mu_B \mathbf{B} \cdot \mathbf{S} + V_{disorder}[\mathbf{x}] \quad (42)$$

where the first term is the kinetic energy of an electron in a magnetic field, the second term is the Coulomb interaction between the electrons, the third term is spin-orbit coupling, and the last term is the potential created by disorder.

In strong magnetic fields, spin-orbit coupling dominates over the Coulomb interaction, and we expect the electrons to be spin-polarized. Therefore we essentially treat  $\mathbf{B} \cdot \mathbf{S}$  as a constant and drop it from the Hamiltonian. In general, electrons may also tunnel between energy eigenstates, which is referred to as Landau level mixing in the present context. Landau level mixing is naturally large when the gap between Landau levels is small, and therefore we neglect it in the strong magnetic field regime since the energy spacing  $\hbar\omega_c \propto B$  is large. We do not consider the effect of the disorder potential because as in the treatment of the IQH effect, disorder is not relevant to electron dynamics or essential physics, but rather the finite width of the Hall plateaus. In other words we first develop the electron dynamics in the absence of disorder, and then invoke it afterwards when discussing the plateaus. The only terms that remain are the kinetic energy and

Coulomb interaction

$$H = \frac{1}{2m} \sum_{j=1}^N \mathbf{\Pi}_j^2 + \sum_{k < j} \frac{e^2}{4\pi\epsilon_0 |\mathbf{x}_j - \mathbf{x}_k|}. \quad (43)$$

We restrict our attention to the LLL where the kinetic energy becomes an irrelevant constant. Formally, we restrict the Coulomb interaction to the LLL using projectors  $\mathcal{P}_{LLL}$ , and the Hamiltonian becomes [7]

$$H = \mathcal{P}_{LLL} \sum_{k < j} \frac{e^2}{4\pi\epsilon_0 |\mathbf{x}_j - \mathbf{x}_k|} \mathcal{P}_{LLL} \quad (44)$$

which can be expanded explicitly but further manipulations have not proved fruitful.<sup>2</sup> Therefore the conventional route is to instead project the wave functions onto the LLL. The result is equivalent, but the wave function approach is cleaner.

## 2.2 Laughlin states

We follow the reasoning of Laughlin to arrive at his ansatz wave function using a first-principles approach provided in [9]. Recall that the LLL single-electron wave function in the symmetric gauge can be expressed as

$$\psi(\mathbf{r}) = f(z) e^{-\frac{1}{4}|z|^2} \quad (45)$$

where  $f(z)$  is a polynomial in the variable  $z = x + iy$ . Note that  $\psi(\mathbf{r})$  itself is not a holomorphic function since the exponential term depends on  $\bar{z}$ . Also the requirement that  $f(z)$  is a polynomial is hinged on restricting the wave function to the LLL. The  $N$ -electron wave function can be constructed by taking the Slater determinant of the single-particle wave function to obtain<sup>3</sup>

$$\psi[\mathbf{r}] = f[z] e^{-\frac{1}{4} \sum_{i=1}^N |z_i|^2} \quad (46)$$

where

$$f[z] = \begin{vmatrix} z_1^0 & \dots & z_N^0 \\ \vdots & \ddots & \vdots \\ z_1^{N-1} & \dots & z_N^{N-1} \end{vmatrix} = \prod_{i < j}^N (z_i - z_j). \quad (47)$$

The Slater determinant is used to construct an antisymmetrization of a product state wave function. In our case, each orbital corresponds to an angular momentum value  $m$ , which is simply the power of  $z_i$ . We use the notation  $[z] = (z_1, \dots, z_N)$ ,  $[\mathbf{r}] = (\mathbf{r}_1, \dots, \mathbf{r}_N)$  to denote the positions of the  $N$  particles. It is clear that the wave function is antisymmetric under particle exchange as is required for a system of fermions. In other words,  $f[z] \mapsto -f[z]$  under the exchange of particle coordinates  $z_i \leftrightarrow z_j$  ( $i \neq j$ ). In addition,  $f[z]$  is a homogenous polynomial in the variable  $z_i$ , and the highest power of any  $z_i$  that appears is  $N - 1$ . Consequently the state  $\psi[\mathbf{r}]$  corresponds to the case where all the states from  $m = 0$  to  $m = N - 1$  are occupied, and therefore the filling factor is  $\nu = 1$ . By fully filling the LLL, we have constructed the  $N$ -electron wave function without considering the Coulomb interaction at all as is the case for the IQH effect. It turns out that this wave function is the unique state of any two-body interaction potential in the LLL which both maximizes the electron density and minimizes the total angular momentum.

---

<sup>2</sup>Note that we cannot utilize perturbation theory since the Coulomb interaction is the only interaction involved.

<sup>3</sup>This wave function is only equal to the actual wave function up to some irrelevant constants.

We now consider the case of a partially filled LLL,  $\nu < 1$ . Laughlin first postulated the ansatz

$$\psi(\mathbf{r}) = f[z] e^{-\frac{1}{4} \sum_{i=1}^N |z_i|^2}, \quad f[z] = \prod_{i < j} f(z_i - z_j) \quad (48)$$

and then restricted the form of  $f(z)$  due to first-principles considerations. As before  $\psi(\mathbf{r})$  must be antisymmetric upon particle exchange and therefore  $f(z)$  must be odd. Due to conservation of angular momentum, we require that  $f[z]$  is a homogenous polynomial of degree  $M$  where  $M$  is the total angular momentum. This restricts the form to  $f(z) = z^m$  for some odd positive integer  $m$ , and thus we have

$$f[z] = f_m[z] = \prod_{i < j}^N (z_i - z_j)^m \quad (49)$$

and denote the corresponding wave function by  $\psi_m(\mathbf{r})$ . We will show that  $\psi_m(\mathbf{r})$  is the (approximate) eigenstate of the  $\nu = 1/m$  filling factor. Note that each electron coordinate  $z_i$  has maximum degree  $M = m(N - 1)$  which represents the maximum angular momentum that the electron may possess.

### 2.3 Plasma analogy

We now provide a well-known proof that  $\nu = 1/m$  in the thermodynamic limit of the Laughlin state [9, 4]. We write the Laughlin state as a Boltzmann factor

$$|\psi_m[z]|^2 = e^{-\beta\Phi}, \quad \beta = 2/m, \quad \Phi = m^2 \sum_{i < j} (-\ln |z_i - z_j|) + \frac{m}{4} \sum_k |z_k|^2. \quad (50)$$

It is not very difficult to see that the wave function can be written in this form, but it is enlightening to note that the potential energy  $\Phi$  has a physical interpretation. To understand the first term of  $\Phi$ , note that for a 2-dimensional electron gas, the electric potential of charge  $m$  particles can be written

$$\phi(\mathbf{r}) = m(-\ln(r/r_0)) \quad (51)$$

and a group of such particles has potential energy

$$U = m^2 \sum_{i < j} (-\ln |z_i - z_j|). \quad (52)$$

To understand the second term, let  $\phi(\mathbf{r}) = \frac{1}{4}|z|^2$  and note that the charge density that corresponds to this electric potential is

$$\nabla \cdot \mathbf{E} = -\nabla^2 \phi = -1/l^2 = 2\pi\rho_B \quad (53)$$

where  $\rho_B = -1/2\pi l^2$  is a constant negative charge density. Hence the second term of  $\Phi$  corresponds to a constant background of charge  $m$  particles with density  $\rho_B$ . Since  $2\pi l^2$  is the area enclosed by one flux quantum, the background charge is precisely the density of flux quanta in units of flux quantum. We see that the wave function  $\psi_m[z]$  corresponds to a plasma of  $N$  particles with charge  $m$ . Note however that since we are dealing with an electron gas, this is not the physical charge of the electron but more of a mathematical tool. It will be of central importance when considering excitations of the electron gas.

## 2.4 Excitations

Now that we understand the wave function of the  $\nu = 1/m$  filling factor, we consider excitations of this state by removing and adding electrons [4, 7]. We first consider the simple example of removing a single electron (or adding a hole) from the  $m = 0$  orbital localized at the origin. We posulate an ansatz [9]

$$\psi_{hole,m}[z, Z] = \left( \prod_{i=1}^N z_i \right) \psi_m[z]. \quad (54)$$

Note that  $\psi_{hole,m}[z]$  vanishes when any electron coordinate  $z_i$  approaches 0 and therefore the electron density at the origin is 0 as intended. For  $\nu = 1$  ( $m = 1$ ), we refer to the absence of an electron as a hole, and for  $\nu \neq 1$  ( $m > 1$ ) we refer to it as a quasi-hole. We will see that holes and quasiholes have different properties. The insertion of the hole term  $\prod z_i$  creates a so-called vortex in the wavefunction at the origin. We will see in later sections that electrons encircling this vortex gain a phase. We will also see how to physically realize this vortex through the adiabatic insertion of a flux quantum through a slim flux tube.

We generalize this ansatz to remove  $M$  electrons at positions  $Z_k$  from the  $\nu = 1/m$  state

$$\psi_{holes,m}[z, Z] = \left( \prod_{j=1}^M \prod_{i=1}^N (z_i - Z_j) \right) \psi_m[z]. \quad (55)$$

We return to the plasma analogy to identify the charge associated with these quasiholes. We consider a single quasi-hole centered at  $Z$  and write the wave function as a Boltzmann factor

$$|\psi_{hole}[z, Z]|^2 = e^{-\beta \Phi'}, \quad \Phi' = \Phi - m \sum_{i=1}^N \ln |z_i - Z|. \quad (56)$$

The addition term corresponds to an impurity of unit charge located at  $Z$ . As before, the plasma analogy suggests that the thermodynamic limit of the system corresponds to an interacting plasma of charge  $m$  particles with a uniform positive background density  $\rho_B$ , and the addition of an impurity of unit charge located at  $Z$ . The dynamics of a plasma are controlled by the affinity to lower its energy by reaching charge neutrality. The introduction of a positive impurity requires that the plasma (which consists of positively charged particles) moves away from the impurity. Since each plasma particle has charge  $m$  and the impurity has charge 1, a net reduction of  $1/m$  plasma particles is required to screen the impurity. However as mentioned before, the charge  $m$  of the plasma particles is not a physical charge, and since the true particles are electrons of charge 1, the reduction of  $1/m$  plasma particles implies that the quasi-hole has charge  $1/m$  in units of electron charge. A similar argument can be used to explain the addition of an electron at position  $Z$  with the state given by<sup>4</sup>

$$\psi_{electron,m}[z, Z] = \prod_{i=1}^N \left( 2 \frac{\partial}{\partial z_i} - \bar{Z} \right) \psi_m[z]. \quad (57)$$

This particle excitation is known as a quasielectron. Using the plasma analogy, it can be shown that the quasielectron has charge  $-1/m$ . The wave function form of the quasielectron is more difficult to deal with than that of the quasi-hole, and therefore we will primarily deal with the latter excitation.

---

<sup>4</sup>The derivative only acts on the polynomial factor of  $\psi_m[z]$

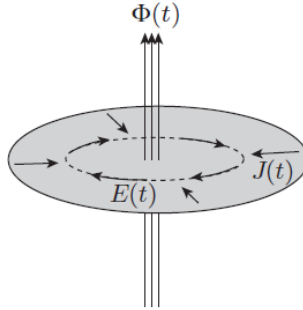


Figure 4: Construction of Laughlin quasielectron by adiabatically inserting a  $\Phi_0$ -flux tube [4].

## 2.5 Flux tubes

We will now see how the Hall conductivity and fractional charge of quasiholes are related through an elegant physical argument proposed by Laughlin [4, 7, 3]. Consider introducing a slim tube of magnetic flux, or flux tube, to the 2-dimensional electron gas at a position  $Z$ . The flux tube initially carries no flux and is then adiabatically increased to one flux quantum  $\Phi_0$ . The only interaction between the flux tube and electrons is the Aharonov-Bohm effect. Since at the end of adiabatic flux insertion the flux is exactly one flux quantum, electrons orbiting the flux tube gain a phase of  $2\pi$  which can be removed through a gauge transformation. In other words, the Hamiltonian after flux insertion is physically equivalent to the initial Hamiltonian. Due to the presence of an energy gap in the bulk of the system, we expect that the ground state remains an eigenstate after flux insertion. However it will not remain in the ground state as we will see since an excitation has been created. To see how this excitation is manifested, first recall Faraday's law which implies that an electric field is induced due to the change in magnetic flux

$$\oint_Z d\mathbf{l} \cdot \mathbf{E} = -\frac{d\Phi}{dt}. \quad (58)$$

where  $\Phi$  is the flux contained by the flux tube, and the integral is carried out over a curve enclosing the flux tube. Since the flux tube is a slim cylinder, the induced electric field is concentric about the flux tube, and its strength only depends on the radial distance  $r$ , or written explicitly

$$\mathbf{E}(t) = -\frac{1}{2\pi r} \frac{d\Phi}{dt} \hat{\phi}. \quad (59)$$

This electric field induces a radial current  $\mathbf{J}(t)$  towards the flux tube

$$\mathbf{J}(t) = \boldsymbol{\sigma} \cdot \mathbf{E}(t). \quad (60)$$

We can compute the net charge transported to  $Z$  through this induced current

$$Q = \int_0^T dt \mathbf{J}_{total}(t) = \sigma_{xy} \int_0^T dt \oint_Z d\mathbf{l} \cdot \mathbf{E} = -\sigma_{xy} \Phi_0 = -\frac{q}{m} \quad (61)$$

where in the last equality we used that  $\sigma_{xy} = \nu e^2/h = e^2/(hm)$ . Remarkably the charge accumulated at  $Z$  is precisely the charge of a quasielectron. The insertion of a flux tube and adiabatic increase of its flux  $0 \mapsto \Phi_0$  creates a quasielectron centered at the point of flux insertion. From this argument it is evident that a quasielectron can be viewed as the combination of a particle of

charge  $q/m$  and a  $\Phi_0$ -flux tube. This flux tube is essential to understanding the dynamics of this composite particle.

## 2.6 Fractional statistics of Laughlin state

We now explore the exchange statistics of the Laughlin state, whose quasielectron excitations we now view as composite objects of flux tubes and fractionally charged particles called composite fermions [3, 4, 7]. We first consider a simplified model consisting of two particles of charge  $q$  bound to antipodal points of a ring. The only degree of freedom in this system is the joint rotation of the particles described by an angle  $\phi$ . The Hamiltonian is given by

$$H = \frac{L^2}{2I} = \frac{\hbar^2}{2I} \left( -i \frac{\partial}{\partial \phi} \right)^2 \quad (62)$$

with eigenstates and energy levels

$$\psi(\phi) = e^{im\phi}, \quad \varepsilon_m = \frac{(\hbar m)^2}{2I} \quad (63)$$

where  $I$  is the moment of inertia,  $L$  is the angular momentum, and  $m$  is in general any real number. For bosons and fermions,  $m$  must be an integer. Note that particle exchange amounts to the phase translation  $\phi \mapsto \phi + \pi$  which may flip the sign of the wave function depending on the parity of  $m$ . For bosons,  $m$  must be even and for fermions  $m$  must be odd. We now consider the insertion of a flux tube with flux  $\Phi$  (or  $\Phi$ -flux tube) into each particle. We assume that each particle cannot experience the effect of its own flux tube. The Hamiltonian can be written

$$H' = \frac{\hbar^2}{2I} \left( -i \frac{\partial}{\partial \phi} + \frac{\theta}{\pi} \right)^2, \quad \theta = \pi \frac{q}{e} \frac{\Phi}{\Phi_0} \quad (64)$$

and the energy levels are

$$\varepsilon'_m = \frac{\hbar^2}{2I} \left( m + \frac{\theta}{\pi} \right)^2. \quad (65)$$

Under exchange, the two-particle system gains a phase  $e^{i\theta}$  in addition to the boson/fermion exchange phase  $e^{i\pi m} = \pm 1$ . For non-integral values of  $\theta/\pi$ , it is clear that the effective particles are not fermions or bosons since they gain a fractional angle upon exchange. Particles with such fractional statistics are known as (abelian) anyons.

We now return to the case of the Laughlin quasielectron (quasi-hole) and its exchange statistics. Recall that a quasielectron (quasi-hole) at filling factor  $\nu = 1/m$  is the combination of a fractional charge  $q = \mp e/m$  and a  $\Phi_0$ -flux tube. We can use the above formalism to obtain that the statistics of the quasielectron (quasi-hole) is determined by  $\theta = \pm \pi/m$ . However we did not include the Aharonov-Bohm phase in the above model. Therefore the total phase due to exchange is

$$\theta = \frac{\pi}{m} \left( \frac{\Phi}{\Phi_0} \pm 1 \right) = \frac{\pi}{m} \cdot \frac{B^* A}{\Phi_0} \quad (66)$$

where  $\Phi$  denotes the magnetic flux enclosed by the orbit. The first term corresponds to the applied magnetic field, and the second term corresponds to the flux tube. We see that there is a new effective magnetic field  $B^*$  whose magnitude relative to the applied field  $B$  depends on the sign of flux tube attachment, or whether the particle encircles a quasi-hole or quasielectron. The flux of a

quasielectron (quasihole) is therefore oriented parallel (antiparallel) to the applied magnetic field. To intuitively understand why the flux tube of a quasihole is oriented antiparallel to the magnetic field, consider the effect of increasing the strength of the magnetic field while holding the filling factor  $\nu$  constant. The magnetic length decreases which increases the electron density  $n_e = \nu/2\pi l^2$  and the Aharonov-Bohm phase. Therefore the removal of an electron (insertion of quasihole) should be associated with a decrease in the magnetic field, which is precisely the result we derived above.

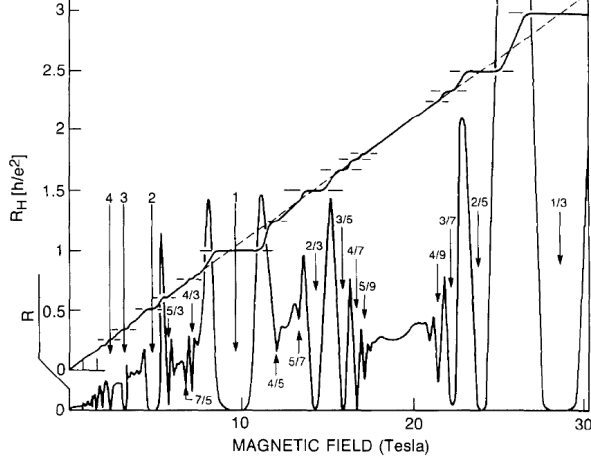


Figure 5: Hall plateaus at numerous filling factors  $\nu = p/q$  ( $q$  odd) measured in a clean 2-dimensional semiconductor electron gas [12]. These are located both in the LLL ( $0 < \nu < 1$ ) as well as higher Landau levels  $\nu > 1$ . There is a small dip in longitudinal resistance at  $\nu = 1/2$  (an even denominator state).

## 2.7 Composite fermions

In the previous sections, we discussed the perspective of excitations of Laughlin states as the bound state of a fractionally charged particle with a  $\Phi_0$ -flux tube piercing through it, a so-called composite fermion. We will now further develop this theory as derived in [7, 4]. Throughout this section we write the polynomial part of the  $\nu = 1/m$  Laughlin state  $\psi_m$  as  $f_m$ . Consider the Laughlin state at filling factor  $\nu = 1/(2p+1)$  where  $p$  is a non-negative integer

$$f_{2p+1} = \prod_{i < j}^N (z_i - z_j)^{2p+1} = \prod_{i' < j'}^N (z'_i - z'_j)^{2p} \prod_{i < j}^N (z_i - z_j). \quad (67)$$

In the second equality we simply split the factor into two independent products. The second factor is the Vandermonde polynomial which describes the  $\nu = 1$  IQH state. The first factor is very similar to the vortex created when constructing the quasihole state, except that in the present case  $2p$  vortices are bound to each electron (not a fixed position). We refer to this quasielectron consisting of an electron and an even number of quantized vortices as a composite fermion. We interchangeably use the term vortices and flux tubes. Although vortices are a property of the wave function, and flux tubes are a physical object, the two are said to be topologically similar in that they both produce a phase change in electrons orbiting them. We interchangeably use the term flux tube and vortex when referencing this phase change. It is quite natural that an even number of flux tubes is required to produce a composite fermion. It results from the same reasoning that

the denominator of the Laughlin filling factor  $\nu = 1/m$  is odd (the antisymmetry requirement of fermions).

From this perspective, we see that the first factor transforms the electrons into composite fermions by bounding  $2p$  flux tubes to each one, and the second term then forms a  $\nu = 1$  integer quantum Hall phase of these composite fermions. It is crucial to note that the integer quantum Hall phase is not one of electrons but of composite fermions. In a mean field approximation, we can treat the flux bound to each electron as static and partially cancel out the original magnetic field. The resulting state would then describe a sea of non-interacting composite fermions in a reduced magnetic field. As derived earlier, the effective magnetic field is

$$B^* = B \pm 2pn_e\Phi_0. \quad (68)$$

While the effective magnetic field  $B^*$  that the composite fermions experience is in general different from that of the applied field  $B$ , the physical field remains  $B$ . In other words, measuring the magnetic field at the sample using a typical electron-based measuring device would yield  $B$ .

We have used two tools for understanding composite fermions: vortices and flux tubes. Neither of these pictures are entirely accurate. The flux tube picture is a bit misleading since composite fermions are not literally bound states of electrons and magnetic flux tubes, although it is helpful to think of it this way. The flux tubes derive from a so-called Chern-Simons gauge field rather than the magnetic field. We will not cover this gauge theory for brevity, but it is important to note of its existence.

## 2.8 Jain sequences

As mentioned in the previous section, composite fermions experience an effective magnetic field [7, 4] and therefore experience

$$N_\Phi^* = N_\Phi \pm 2pN = N \left( \frac{1}{\nu} \pm 2p \right) \quad (69)$$

flux quanta where  $N_\Phi = \Phi/\Phi_0$  is the number of flux quantum penetrating the sample, and the electron filling factor is  $\nu = N/N_\Phi$ . The  $\pm 2p$  corresponds to attaching  $2p$  flux quanta to each electron parallel (antiparallel) to the magnetic field. We have the composite fermion filling factor

$$\nu^* = \frac{N}{N_\Phi^*} = \frac{1}{1/\nu \pm 2p}. \quad (70)$$

The number of composite fermions is equal to the number of electrons, since we are only attaching flux tubes to a single electron to obtain a composite fermion. However since the effective magnetic field is different, the resulting composite fermion filling factor is also different. If we insert flux tubes antiparallel to the magnetic field then the effective magnetic field reduces and the composite fermion filling factor is greater than the electron filling factor. If we place the composite fermions with  $2p$ -flux tubes in the IQH phase  $\nu^* = n$  then the corresponding electron filling factor can be written as

$$\nu = \frac{n}{2pn \mp 1} < 1. \quad (71)$$

Note that when stating the composite fermion filling factor, it is necessary to also provide the order of the flux tubes. We have two sequences of electron filling factors corresponding to parallel or antiparallel attachment ( $\pm$ ). For instance, if we let  $p = 2$  then we have  $\nu = 1/5, 2/7, 3/9, \dots$  for parallel attachment (+) and  $\nu = 1/3, 2/5, 3/7, \dots$  for anti-parallel attachment (-). These sequences

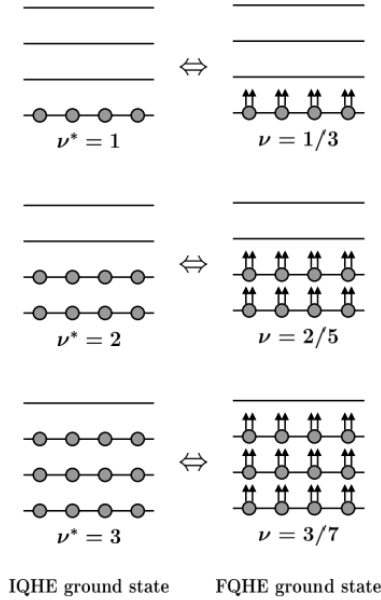


Figure 6: Schematic showing how the relationship between composite fermion Lambda levels and their filling factors  $\nu^*$  (left), and their corresponding filling electron filling factors (right) [7]. There are 2 flux tubes attached to each electron to form a composite fermion.

of electron filling factors are known as Jain sequences, and it turns out that the Hierarchy states are strongest at these filling factors.

The statistics of composite fermions are trivial since the statistics angle is  $\theta = 2p\pi = 0 \bmod 2\pi$ , and so exchange of composite fermions yields trivial phase  $\eta = e^{i\theta} = 1$ . Consequently, as the name suggests, composite fermions are fermions as the flux tubes do not endow them with nontrivial anyonic exchange properties. However, excitations of composite fermions are anyonic.

## 2.9 Lambda levels

Within the partially filled LLL, we have found that electrons transform into composite fermions at particular filling fractions, and these composite fermions form an IQH phase [7]. In other words, the LLL has split into so-called Lambda levels of composite fermions indexed by the composite fermion filling factor  $\nu^*$ . If we add an electron to a sea of composite fermions, it will transform into a composite fermion. To see this, we must understand why electrons favor transforming into composite fermions. The explanation is quite simple. Electrons in a fractionally-filled Landau level strongly interact through Coulomb repulsion. By adiabatically inserting magnetic flux, the resulting composite fermions interact weakly, and therefore the energy of the system decreases.

## 2.10 Halperin bilayer state

Introducing new degrees of freedom can increase electron correlations and lead to novel quantum phases. Halperin considered the addition of a degree of freedom and considered electron correlations through this degree of freedom [7]. Such degrees of freedom include spin, valley (which we will discuss later), and layer. Surprisingly, the layer degree of freedom was not intended by Halperin during the inception of his multi-component FQH phase. Nonetheless we interpret the result

through a more modern perspective and consider a bilayer system which we will return to when we discuss bilayer graphene. There is one important parameter to consider when analyzing electron correlations, the ratio of interlayer to intralayer electron correlations  $d/l$  where  $d$  is the spacing between the layers and  $l$  is the magnetic length. In the limit  $d/l \rightarrow \infty$  we expect zero interlayer electron correlations while for  $d/l \rightarrow 0$  the problem becomes identical to that of a single layer with spinful electrons. In the former limit, we can generalize Laughlin states to include the layer degree of freedom

$$\psi_{mn} = \prod_{i < j} (z_i - z_j)^m \prod_{r < s} (w_r - w_s)^n \quad (72)$$

where  $z$  denotes the coordinates on one layer and  $w$  that of the other layer. In the intermediate regime  $d/l \neq 0$ , we expect exciting quantum phases. Halperin generalized the Laughlin state to

$$\psi_{m'm''m} = \prod_{i < j} (z_i - z_j)^{m'} \prod_{r < s} (w_r - w_s)^{m''} \prod_{g,h} (z_g - w_h)^m \quad (73)$$

where he included the factor  $\prod(z_g - w_h)^m$  representing interlayer electron correlations.

## 2.11 Moore-Read state

Thus far we have only considered odd-denominator filling factors. Recall that the origin of this odd-denominator requirement is the Pauli exclusion principle of electrons. If the denominator were even then the state would not describe fermions. Nonetheless the  $\nu = 1/2, 5/2$  and other even-denominator states have been observed [7]. None of the approaches considered so far can be used to explain these states. Moore and Read showed that the  $\nu = 1/2$  state can be described by [7]

$$\psi_2 = \prod_{i < j} (z_i - z_j)^2 \text{Pf} \left( \frac{1}{z_i - z_j} \right) \quad (74)$$

where Pf is the Pfaffian. The derivation involves conformal field theory which is outside the scope of this paper and may provide a framework to understanding other FQH phases. Numerical simulations show great evidence that this state describes the  $\nu = 1/2, \nu = 5/2$  filling factors. The state describes a  $p$ -wave superconductor paired state with fractional charge  $e/4$ . Apart from being interesting in its own right, the  $\nu = 1/2, 5/2$  states are degenerate and the quasielectrons are so-called nonabelian anyons. That is to say braiding the quasielectrons does not introduce a U(1) scalar phase but a U( $n$ ) factor where the operator acts in the  $n$ -dimensional degenerate eigenspace. This makes the  $\nu = 1/2, 5/2$  highly sought after due to their application to topological quantum computing, a field which utilizes the global nature of the braiding of nonabelian anyons for (local) noise-insensitive quantum computation. The particle-hole conjugate of the Moore-Read Pfaffian state is the so-called anti-Pfaffian state which is topologically distinct. There is debate over which state is favored in certain FQH phases. It turns out that the Moore-Read  $\nu = 5/2$  state is a specific case of the more general Read-Rezayi states which have also been sought after for their nonabelian anyon quasielectrons.

## 3 Bilayer Graphene

We have now covered the integer and fractional quantum Hall effects and are ready to understand their manifestation in bilayer graphene. We will first explore monolayer graphene and derive its band structure and integer quantum Hall effect as an introduction into the analysis. We will then

perform the same analysis for bilayer graphene. The intent is to replicate experimental data with our numerical simulations to better understand the band structure of bilayer graphene.

### 3.1 Monolayer graphene

We now describe the movement of electrons in the graphene lattice which we model as electrons hopping between orbitals on the lattice sites. This description is known as the tight-binding model and can provide very powerful insight on electron dynamics. Note however that it neglects inter-electron interactions. Graphene is a honeycomb lattice with two atoms in the unit cell, or the (non-unique) region in space with minimal area which can be used to tile the whole lattice. The honeycomb lattice can be considered as two triangular lattices translated with respect to one another. We attribute a sublattice index  $\alpha$  to each of the two atoms in the unit cell. The primitive lattice vectors, or the vectors which connect the origin to the two distinct sublattice vertices can be written as [4]

$$\mathbf{a}_1 = \boldsymbol{\tau}_3 - \boldsymbol{\tau}_2 = \sqrt{3}a_c(1, 0), \quad \mathbf{a}_2 = \boldsymbol{\tau}_1 - \boldsymbol{\tau}_2 = \frac{\sqrt{3}}{2}a_c(1, \sqrt{3}) \quad (75)$$

where

$$\boldsymbol{\tau}_1 = a_c(0, 1), \quad \boldsymbol{\tau}_2 = -\frac{a_c}{2}(\sqrt{3}, 1), \quad \boldsymbol{\tau}_3 = \frac{a_c}{2}(\sqrt{3}, -1) \quad (76)$$

are the nearest-neighbor hopping vectors and  $a_c \approx 1.42\text{\AA}$  is the carbon-carbon spacing. The lattice vectors, or the positions of the atoms can then be expressed as

$$\mathbf{R}_\alpha = n_1 \mathbf{a}_1 + n_2 \mathbf{a}_2 + \boldsymbol{\tau}_\alpha, \quad n_1, n_2 \in \mathbb{Z} \quad (77)$$

where we use the convention  $\boldsymbol{\tau}_A = \mathbf{0}$ ,  $\boldsymbol{\tau}_B = -\boldsymbol{\tau}_3$ .

It is natural to perform the same analysis for the Fourier (momentum) space analog of the lattice, or the so-called reciprocal lattice. The reciprocal lattice has primitive vectors  $\mathbf{b}_j$  ( $j = 0, 1$ ) so that  $\mathbf{a}_i \cdot \mathbf{b}_j = 2\pi\delta_{ij}$ . This momentum space lattice intuitively represents electron states in momentum space rather than real space. An important region in the reciprocal lattice is the so-called Brillouin zone (BZ) as every momentum in the reciprocal lattice is equivalent to some momentum in the Brillouin zone (modulo a reciprocal lattice vector). We compute the primitive reciprocal vectors

$$\mathbf{b}_1 = \frac{2\pi}{3a_c}(\sqrt{3}, -1), \quad \mathbf{b}_2 = \frac{4\pi}{3a_c}(0, 1). \quad (78)$$

We assume the graphene lattice sites have localized electron orbitals, known as Wannier orbitals, and we define the creation and annihilation operators of these orbitals as  $|n, \mathbf{R}\rangle = c_{n, \mathbf{R}}^\dagger |0\rangle$  where  $n$  is the orbital index and  $\mathbf{R}$  is the lattice site. For the computation below, we only consider a single orbital on each lattice site, and so we drop the orbital index. Since these are electron operators, they obey the anticommutation relations [4]

$$\{c_m, c_n^\dagger\} = c_m c_n^\dagger + c_n^\dagger c_m = \delta_{mn}, \quad \{c_m, c_n\} = \{c_m^\dagger, c_n^\dagger\} = 0, \quad (79)$$

as required by antisymmetry.

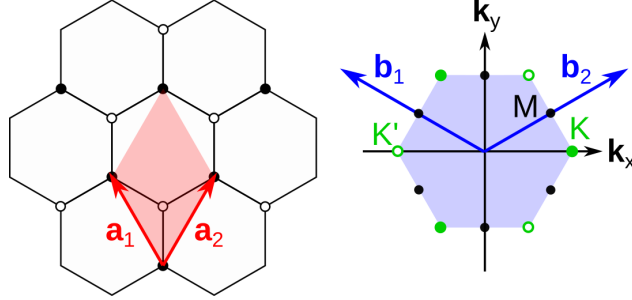


Figure 7: Graphene primitive unit vectors ( $\mathbf{a}_1, \mathbf{a}_2$ ) and the primitive unit cell shaded red (left). Graphene primitive reciprocal vectors ( $\mathbf{b}_1, \mathbf{b}_2$ ) and the Brillouin zone shaded blue (right). The  $\mathbf{K}, \mathbf{K}'$  points are colored green [11].

### 3.1.1 Tight-binding model

We can write the nearest-neighbor tight-binding Hamiltonian

$$H = -\gamma_0 \sum_{\langle \mathbf{R}_A^i, \mathbf{R}_B^j \rangle} (c_{\mathbf{R}_A^i}^\dagger c_{\mathbf{R}_B^j} + h.c.) \quad (80)$$

where *h.c.* denotes the Hermitian-conjugate of the prior term ( $a+h.c. = a+a^\dagger$ ), and  $\gamma_0$  is the hopping amplitude. The sum is carried over nearest neighbor lattice sites. Although this Hamiltonian may appear complicated, each term merely describes the hopping of an electron between lattice sites. The factor  $c_{\mathbf{R}_A^i}^\dagger c_{\mathbf{R}_B^j}$  describes an electron hopping from the  $\mathbf{R}_B^j$  site to the  $\mathbf{R}_A^i$  since it is being annihilated from the former site and created at the latter site. We now transform this Hamiltonian into momentum space via a Fourier transform

$$c_{\mathbf{R}_A^i}^\dagger = \frac{1}{\sqrt{N}} \sum_{\mathbf{k} \in \text{BZ}} e^{-i\mathbf{k} \cdot \mathbf{R}_A^i} c_{\mathbf{k}, \alpha}^\dagger \quad (81)$$

where  $N$  denotes the number of unit cells. The  $AB$  term can be computed

$$-\gamma_0 \sum_{\langle \mathbf{R}_A, \mathbf{R}_B \rangle} c_{\mathbf{R}_A}^\dagger c_{\mathbf{R}_B} = -\gamma_0 \sum_{\mathbf{k}} \sum_{i=1}^3 e^{-i\mathbf{k} \cdot \boldsymbol{\tau}_i} c_{\mathbf{k}, A}^\dagger c_{\mathbf{k}, B}, \quad (82)$$

and the  $BA$  term is simply its Hermitian-conjugate. The momentum space tight-binding Hamiltonian can therefore be written as

$$H(\mathbf{k}) = \begin{pmatrix} 0 & -\gamma_0 f(\mathbf{k}) \\ -\gamma_0 f(\mathbf{k}) & 0 \end{pmatrix}, \quad f(\mathbf{k}) = \sum_{j=1}^3 e^{-i\mathbf{k} \cdot \boldsymbol{\tau}_j} \quad (83)$$

in the basis  $\{c_{\mathbf{k}, A}^\dagger, c_{\mathbf{k}, B}^\dagger\}$ . We have the energy eigenvalues

$$\varepsilon_{\pm 1, \mathbf{k}} = \pm \gamma_0 |f(\mathbf{k})| \quad (84)$$

where  $\pm 1$  corresponds to the conduction and valence bands respectively. The valence and conduction bands intersect at reciprocal lattice sites, forming so-called Dirac cones. There are six corners of the Brillouin zone, with half corresponding to each “reciprocal sublattice”. To distinguish be-

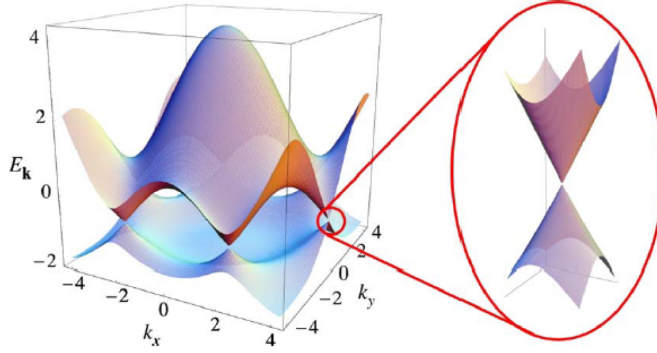


Figure 8: Band structure of monolayer graphene intersecting at  $\mathbf{K}, \mathbf{K}'$  valleys forming Dirac cones [5].

tween the sublattice of the real space and that of the reciprocal space, we use the term valley, denoted  $\eta = \pm 1$ , to refer to the latter. There are two valleys in the BZ which can be represented by reciprocal lattice vectors

$$\mathbf{K} = \frac{4\pi}{3\sqrt{3}a_c}(1, 0), \quad \mathbf{K}' = -\mathbf{K} \quad (85)$$

as representatives of valley  $\eta = \pm 1$  respectively. These sites are called Dirac points and are precisely where the valence and conduction bands intersect. We now formulate a low-energy continuum model of graphene by expanding the Hamiltonian about these Dirac points. We take the momenta  $\mathbf{k}$  to be a continuous set in the BZ which eliminates the notion of a lattice. For each valley, we Taylor expand the off-diagonal entries of the tight-binding Hamiltonian (83) to first-order

$$f(\mathbf{k} + \mathbf{K}) \approx -\frac{3a_c}{2}(k_x + ik_y), \quad f(\mathbf{k} + \mathbf{K}') \approx -\frac{3a_c}{2}(k_x - ik_y) \quad (86)$$

where  $|\mathbf{k}| \ll |\mathbf{K}| = |\mathbf{K}'|$  and  $\mathbf{k}$  is measured from the Dirac points. The continuum model Hamiltonian becomes

$$h(\mathbf{k}) = \hbar v_F (\tau_z \sigma_x k_x + \sigma_y k_y) \quad (87)$$

where  $\tau_z$  is the  $\sigma_z$  Pauli matrix acting on the valley subspace ( $\tau_z = \pm 1$  for  $\eta = \pm 1$  respectively), and  $\hbar v_F = \sqrt{3}\gamma_0 a / 2\hbar$  is the Fermi velocity. The conduction and valence bands are given by  $E_{\pm} = \pm v_F |\mathbf{k}|$  respectively. The linearity of this band dispersion reveals that electrons near the Dirac points of graphene behave as though they were relativistic and massless.

### 3.1.2 Magnetic field

We want to study the integer quantum Hall effect in graphene and so we introduce a magnetic field perpendicular to the graphene plane. We first consider the  $\eta = 1$  valley and expand the continuum model Hamiltonian of the previous section [4]

$$h(\mathbf{k})_{\eta=1} = \hbar v_F \begin{pmatrix} 0 & k_x - ik_y \\ k_x + ik_y & 0 \end{pmatrix}. \quad (88)$$

We introduce the effect of a magnetic field  $p_\mu = \hbar k_\mu \mapsto \hbar k_\mu - A_\mu = \Pi_\mu$  where  $A_\mu$  is the magnetic vector potential, and the Hamiltonian becomes

$$h(\Pi)_{\eta=1} = v_F \begin{pmatrix} 0 & \Pi_x - i\Pi_y \\ \Pi_x + i\Pi_y & 0 \end{pmatrix}. \quad (89)$$

Note that the nonzero entries are simply the raising and lowering operators which we defined in our treatment of Landau levels

$$a = \frac{l}{\sqrt{2}\hbar}(\Pi_x + i\Pi_y), \quad a^\dagger = \frac{l}{\sqrt{2}\hbar}(\Pi_x - i\Pi_y), \quad [a, a^\dagger] = 1. \quad (90)$$

The graphene Hamiltonian in a magnetic field can then be written

$$h_{\eta=1} = \sqrt{2}\hbar v_F/l \cdot \begin{pmatrix} 0 & a^\dagger \\ a & 0 \end{pmatrix}. \quad (91)$$

We can analytically solve for the energy levels of this Hamiltonian by considering its square

$$h_{\eta=1}^2 = (\sqrt{2}\hbar v_F/l)^2 \begin{pmatrix} a^\dagger a & 0 \\ 0 & aa^\dagger \end{pmatrix} = (\sqrt{2}\hbar v_F/l)^2 \begin{pmatrix} \hat{n} & 0 \\ 0 & \hat{n}-1 \end{pmatrix} \quad (92)$$

where  $\hat{n} = a^\dagger a$  is the so-called number operator which counts the energy level, or  $\hat{n}|n\rangle = n|n\rangle$ . The energy levels of  $h_{\eta=1}^2$  are simply those of the diagonal energies, and are the squares of that of  $h_{\eta=1}$  and so we have

$$\varepsilon_n = \sqrt{2}\hbar v_F/l \cdot \text{sgn}(n) \sqrt{|n|} \quad (93)$$

and the corresponding eigenstates can be expressed as

$$|n=0\rangle_G^{\eta=1} = \begin{pmatrix} |0\rangle \\ 0 \end{pmatrix}, \quad |n \neq 0\rangle_G^{\eta=1} = \begin{pmatrix} ||n|| \\ \text{sgn}(n) ||n|-1 \rangle \end{pmatrix}. \quad (94)$$

We omit the angular momentum index in the Landau levels. We similarly arrive at the  $\eta = -1$  Hamiltonian

$$h_{\eta=-1} = \sqrt{2}\hbar v_F/l \cdot \begin{pmatrix} 0 & a \\ a^\dagger & 0 \end{pmatrix} \quad (95)$$

which has the same energy levels but the entries of the eigenstates are interchanged. Note that for the ZLL, the eigenstate is completely polarized on the  $A$  sublattice while for all other levels, the eigenstate is split between both sublattices. In addition, each energy level has a degeneracy of 4 due to spin and valley. The spin degeneracy is broken when including Zeeman splitting, and the valley degeneracy can be broken by breaking inversion symmetry.

We now wish to understand the Hall conductivity of graphene. Recall that a fully filled Landau level of electrons (holes) contributes  $\pm e^2/h$  to the Hall conductivity. Therefore if our system is at the charge-neutrality point  $\nu = 0$  so that the positive (negative) levels are occupied by holes (electrons), and the ZLL is split between electrons and holes, then the Hall conductivity cancels to produce 0. If the ZLL of one valley were to be fully occupied, then the Hall conductivity would be  $e^2/2h$ . Thus we have the Hall conductivity sequence

$$\sigma_{xy}^n = 4 \frac{e^2}{h} \left( n + \frac{1}{2} \right), \quad n \in \mathbb{Z} \quad (96)$$

where the  $1/2$  comes from ZLL and the  $4$  is due to spin and valley degeneracies. This sequence was first experimentally observed in 2005 [4].

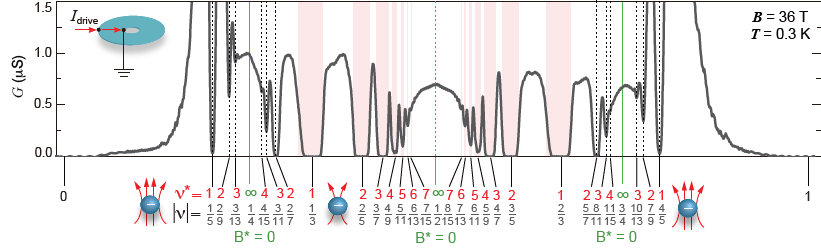


Figure 9: Measured bulk conductance of graphene in Corbino device geometry as a function of filling factor  $0 \leq \nu \leq 1$  at magnetic field  $B = 36\text{ T}$  and temperature  $T = 0.3\text{ K}$ . Note that the plot is fairly symmetric with respect to  $\nu = 1/2$  or  $\nu^* = \infty$ . The top row is the composite fermion filling factor  $\nu^*$  and the bottom row is the corresponding electron filling factor. The smaller integer filling factor  $\nu^*$  dips are stronger [2].

### 3.2 Bilayer graphene

Bilayer graphene consists of two layers of graphene which in the present consideration is separated by a distance of  $3.34\text{\AA}$ . There are two standard stacking arrangements that we must keep in mind. *AA* stacking corresponds with aligned sublattice sites:  $A(B)$  points of one layer on top of  $A(B)$  points of the other. *AB* or Bernal stacking corresponds with the lattice sites of one layer on top of the centers of the honeycombs of the other layer and can be achieved by shifting one layer by a hopping vector  $\tau$ . More explicitly, the lattice sites of the two layers are related

$$\mathbf{R}' = \mathbf{R} + \mathbf{d} \quad (97)$$

where  $\mathbf{d} = 0, \tau_1$  for *AA* and *AB* stacking respectively. We focus our attention to Bernal (*AB*)

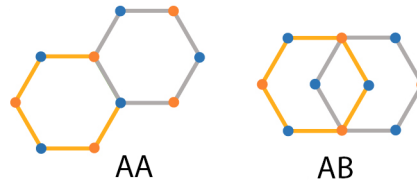


Figure 10: The AA and AB stacking arrangements [1].

stacked bilayer graphene. We have five hopping parameters  $\gamma_0, \gamma_1, \gamma_2, \gamma_3, \gamma_4$  which represent the electron hoppings  $A \leftrightarrow B, A' \leftrightarrow B, A' \leftrightarrow B', A \leftrightarrow B', A \leftrightarrow A'$  respectively. Since both layers are graphene, we assume the intralayer hopping parameters are equal, or  $\gamma_0 = \gamma_2$  and denote it simply as  $\gamma_2$ . Ab initio computations suggest the values  $\gamma_0 = 2.61\text{eV}, \gamma_1 = 361\text{meV}, \gamma_3 = -283\text{meV}$ , and  $\gamma_4 = -138\text{meV}$  [2]. The  $\gamma_3$  term represents trigonal warping and is more important at low magnetic fields. In the following computations, we set  $\gamma_3 = 0$  which introduces minimal errors.

There is an intrinsic interlayer displacement potential  $D_0$  which we do not know the value of a priori. This potential opens up an energy gap which we can measure to deduce its value. We consider an onsite dimer energy  $\Delta' = 15\text{meV}$  raising the energy of  $A'$  and  $B$  relative to  $A$  and  $B'$  which arises to the breaking of inversion symmetry by the hBN substrate. Both nonzero  $\gamma_4$  and

$\Delta'$  break particle-hole symmetry. A similar derivation to that of monolayer graphene shows that

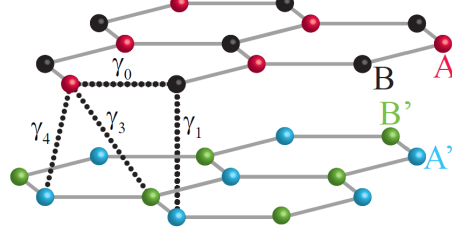


Figure 11: The hopping parameters of our bilayer graphene tight-binding model, and their physical interpretation as hoppings on the bilayer lattice [2].

the tight-binding Hamiltonian of bilayer graphene can be expressed as [2]

$$h(\mathbf{k}) = \begin{pmatrix} u/2 & \gamma_3 f(\mathbf{k}) & \gamma_4 \overline{f(\mathbf{k})} & \gamma_0 \overline{f(\mathbf{k})} \\ \gamma_3 \overline{f(\mathbf{k})} & -u/2 & \gamma_0 f(\mathbf{k}) & \gamma_4 f(\mathbf{k}) \\ \gamma_4 f(\mathbf{k}) & \gamma_0 \overline{f(\mathbf{k})} & -u/2 + \Delta' & \gamma_1 \\ \gamma_0 f(\mathbf{k}) & \gamma_4 \overline{f(\mathbf{k})} & \gamma_1 & u/2 + \Delta' \end{pmatrix} \quad (98)$$

written in the first-quantized orbital basis  $(\varphi_A, \varphi_{B'}, \varphi_{A'}, \varphi_B)$ . We expand this Hamiltonian around the Dirac point to achieve the low-energy Hamiltonian

$$h(\mathbf{k}) = \begin{pmatrix} u/2 & \gamma_3 \pi & \gamma_4 \pi^\dagger & \gamma_0 \pi^\dagger \\ \gamma_3 \pi^\dagger & -u/2 & \gamma_0 \pi & \gamma_4 \pi \\ \gamma_4 \pi & \gamma_0 \pi^\dagger & -u/2 + \Delta' & \gamma_1 \\ \gamma_0 \pi & \gamma_4 \pi^\dagger & \gamma_1 & u/2 + \Delta' \end{pmatrix} \quad (99)$$

where  $\pi = \hbar(k_x - ik_y)$ ,  $\pi^\dagger = \hbar(k_x + ik_y)$ . This expansion comes directly from the low-energy expansion of  $f(\mathbf{k})$  about the Dirac points in the treatment of monolayer graphene. We then introduce a magnetic field to obtain

$$h = \begin{pmatrix} \eta u/2 & \omega_3 a & \omega_4 a^\dagger & \omega_0 a^\dagger \\ \omega_3 a^\dagger & -\eta u/2 & \omega_0 a & \omega_4 a \\ \omega_4 a & \omega_4 a^\dagger & -\eta u/2 + \Delta' & \gamma_1 \\ \omega_0 a & \omega_4 a^\dagger & \gamma_1 & \eta u/2 + \Delta' \end{pmatrix} \quad (100)$$

where  $\omega_0 = \hbar v_F \sqrt{2}/l$  and  $\omega_i = \gamma_i \omega_0 / \gamma_0$  for  $i = 3, 4$ . When switching between valleys  $\eta = \pm 1$ , the basis transforms as  $(\varphi_A, \varphi_{B'}, \varphi_{A'}, \varphi_B) \leftrightarrow (\varphi_{B'}, -\varphi_A, \varphi_B, -\varphi_{A'})$ . The eigenstates of the Hamiltonian take the form

$$|\eta n\rangle_{BG} = \sum_m (c_{\eta n A}^m |m\rangle, c_{\eta n B'}^m |m\rangle, c_{\eta n A'}^m |m\rangle, c_{\eta n B}^m |m\rangle) \quad (101)$$

where  $|m\rangle$  are the usual Landau level orbitals and the  $c_{\eta n X}^m$  are scalars. The energy levels of the Hamiltonian (with  $u = \Delta' = 0$ ) can be approximated as [2]

$$\varepsilon_n \approx \hbar \omega_c \sqrt{n(n-1)}, \quad \hbar \omega_c = \frac{3a_0^2 \gamma_0^2}{2l^2 \gamma_1} \approx \frac{\hbar e B}{m^*} \quad (102)$$

where  $m^* = 0.044 m_e$  is the effective mass of the electron and  $a_0 = \sqrt{3} a_c \approx 2.46 \text{ \AA}$  is the  $AA$

monolayer spacing. For  $B = 6\text{T}$ , we have  $\hbar\omega_c \approx 15.61\text{meV}$ . For  $n = 0$ , the eigenstate is completely polarized on the  $A$  ( $B'$ ) sublattice for  $\eta = \pm 1$  respectively. For  $n = 1$ , the  $\eta = 1$  eigenstate splits between the  $A, A', B$  sublattices

$$|n = 1\rangle_{BG} = \begin{pmatrix} c_A |1\rangle \\ 0 \\ c_{A'} |0\rangle \\ c_B |0\rangle \end{pmatrix} \quad (103)$$

with energy  $\varepsilon_\eta = \omega_0^2/\gamma_1 \cdot (\gamma_4/\gamma_0 + \Delta'/\gamma_1) + \eta\alpha u/2$ . This interplay between sublattice and Landau orbital is partly responsible for the rich bilayer graphene FQH phases we will discuss later.

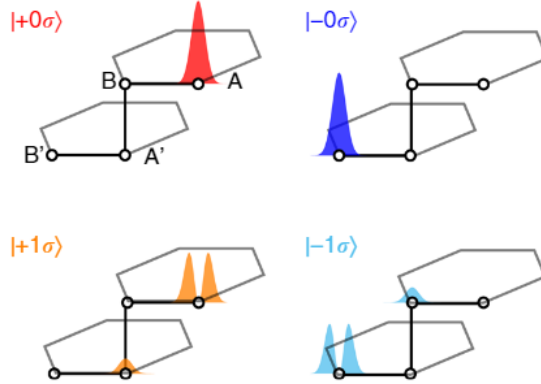


Figure 12: Depiction of wave function of the listed eigenstates  $|\eta n\sigma\rangle$  as residing on the sublattices. For  $|\pm 0\sigma\rangle$ , the state is fully polarized on the  $A, B'$  sublattices respectively. For  $|\pm 1\sigma\rangle$ , the state is partially polarized on the  $A, A'$  and  $B, B'$  sublattices with majority on  $A$  and  $B'$  respectively. A single (double) peak indicates an  $|0\rangle$  ( $|1\rangle$ ) orbital Landau level [6].

We consider the Hall conductivity in the absence of an interlayer potential  $u$ . In this case, the  $n = 0$  and  $n = 1$  states are roughly degenerate, and we consider them as one zero energy state. There is an 8-fold zero energy degeneracy due to this accidental degeneracy as well as the usual 4-fold degeneracy due to spin and valley. We consider the case of negligible Zeeman splitting. Since the valley  $\eta$  only couples to the energies through  $u$ , it does not affect the energies. When we fill the ZLL, by the same argument as the monolayer graphene case, we fill 4 levels above charge neutrality, and any subsequent level adds 4 more levels. Consequently the Hall conductivity sequence becomes

$$\sigma_{xy} = 4\frac{e^2}{h}n, \quad n \in \mathbb{Z}_{\neq 0} \quad (104)$$

with corrections arising from the parameters we neglected above. We see that the accidental ZLL degeneracy removes the  $1/2$  term in  $\sigma_{xy}$  when compared to monolayer graphene.

### 3.3 Scanning tunnelling spectroscopy

We now provide an overview of scanning tunnelling spectroscopy (STS), an experimental method to probe the density of states of 2-dimensional materials using a scanning tunnelling microscope. We follow the derivations in [13]. See Figure 13 for an introduction to the device setup.

At positive tip-sample bias  $V_b$ , electrons may tunnel from the sample to the tip. The probability

(per unit time) of an electron on the tip with wave function  $\psi_\mu$  and energy  $\varepsilon_\mu$  to tunnel to a state in the (top layer of the) sample with wave function  $\psi_\nu$  and energy  $\varepsilon_\nu$  can be expressed as

$$P = \frac{2\pi}{\hbar} |M_{\mu\nu}|^2 \delta(\varepsilon_\mu - \varepsilon_\nu), \quad M_{\mu\nu} = \frac{\hbar}{2m} \int dS (\psi_\mu^* \nabla \psi_\nu - \psi_\nu^* \nabla \psi_\mu) \quad (105)$$

where the integral for the tunnelling matrix element is performed over any surface which separates the tip from the sample. We sum over all states on the tip and sample to obtain the tunnelling current at position  $\mathbf{r}$

$$I(\mathbf{r}, V_b) = \frac{4\pi e}{\hbar} \int_{-\infty}^{\infty} d\varepsilon |M|^2 (f(\mu - eV_b + \varepsilon) - f(\mu - \varepsilon)) \text{LDOS}_S(\mu - eV_b + \varepsilon, \mathbf{r}) \text{DOS}_T(\mu + \varepsilon) \quad (106)$$

where  $V_b$  is the tip-sample bias,  $f(\varepsilon)$  is the Fermi distribution,  $\mu$  is the chemical potential, and we have included a factor of 2 for spin degeneracy. We assume the temperature is sufficiently small so that we can approximate the Fermi distribution as a step function from which we obtain the tunnelling current

$$I(\mathbf{r}, V_b) = \frac{4\pi e}{\hbar} \int_0^{eV_b} d\varepsilon |M|^2 \text{LDOS}_S(\mu - eV_b + \varepsilon, \mathbf{r}) \text{DOS}_T(\mu + \varepsilon) \quad (107)$$

For a sufficiently small tip bias, we can approximate the integral to first order

$$I(\mathbf{r}, V_b) = \frac{4\pi e}{\hbar} V_b |M|^2 \text{LDOS}_S(\mu, \mathbf{r}) \text{DOS}_T(\mu) \quad (108)$$

where  $\mu$  is the Fermi energy. We can then differentiate the current to obtain the differential conductance

$$\frac{dI}{dV_b} = \frac{4\pi e}{\hbar} |M|^2 \text{LDOS}_S(\mu, \mathbf{r}) \text{DOS}_T(\mu) \propto \text{LDOS}_S(\mu, \mathbf{r}). \quad (109)$$

which is proportional to the local density of states. We can obtain the total density of states by sweeping over the sample

$$\text{DOS}(\varepsilon = eV_b) = \frac{1}{Vol} \int d^2\mathbf{r} \text{LDOS}(\varepsilon = eV_b, \mathbf{r}) \quad (110)$$

where  $Vol$  is the volume of the sample, and  $\varepsilon$  is relative to the chemical potential  $\mu$ .

We numerically compute the density of states (DOS) of bilayer graphene and compare our results with those of STS experiment. The DOS counts the number of states at a given energy. In other words, the DOS measures the degeneracy of a given energy level, and for a single band  $\epsilon(\mathbf{k})$ , the DOS is given by [4, 10]

$$\text{DOS}(\varepsilon) = \int_{BZ} \frac{d^2\mathbf{k}}{(2\pi)^2} \delta(\varepsilon - \varepsilon(\mathbf{k})) \quad (111)$$

where  $\delta(x)$  is the Dirac delta function and  $BZ$  denotes the Brillouin zone.<sup>5</sup> We can readily compute this formula given the spectra of the Hamiltonian in the Brillouin zone.

We first compute the density of states in the zero magnetic field regime. The primary parameter

---

<sup>5</sup>When introducing a magnetic field, the Brillouin zone transforms into a new region called the magnetic Brillouin zone, and the density of states integral is carried over this region. Fortunately the Hamiltonian does not depend on momentum  $\mathbf{k}$  and so the integral results in an overall factor applied to the integrand.

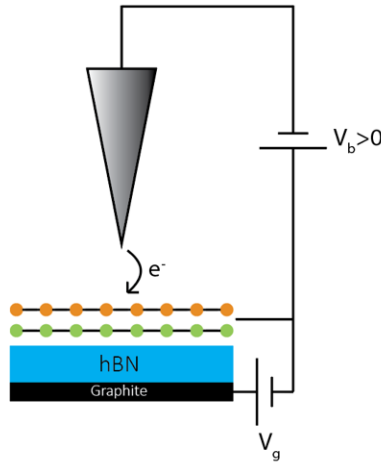


Figure 13: The device arrangement of the scanning tunnelling microscope. The tip is suspended above the sample, and the sample itself resides on a hexagonal boron nitride (hBN) substrate and the back gate makes contact with a graphite substrate. The back gate voltage  $V_g$  controls the electron density and therefore the filling factor on the sample. The tip-sample bias voltage  $V_b$  control the electron tunnelling between the tip and sample. When biased negatively  $V_b < 0$ , electrons tunnel from the sample onto the tip. Since is above the sample, it can only probe electron wave functions on the top layer and is effectively blind to the bottom layer [15].

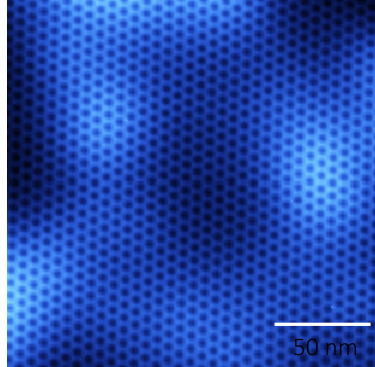


Figure 14: An ultra clean single layer of graphene positioned on top of a hBN substrate with a relative twist angle of  $\sim 1.9^\circ$ , forming a moire superlattice with characteristic length 6.65nm. The scale on the lower right is 50nm. The sample is measured using STM topography in which the bias voltage  $V_b$  is fixed and the vertical height of the tip is swept until a fixed desired value of tunnelling current is obtained [15].

we must consider is the interlayer electric potential  $u$ . Recall that an interlayer potential opens a gap between the valence and conduction bands which we can measure as a gap in the density of states. Since STS is only sensitive to the top layer, the density of states on the top layer becomes

$$\text{DOS}_{AB}(\varepsilon) = \sum_{n\eta\sigma} \int_{\text{BZ}} \frac{d^2\mathbf{k}}{(2\pi)^2} \delta(\varepsilon - \varepsilon_{n\eta\sigma}(\mathbf{k})) \beta_{\eta n}, \quad \beta_{\eta n} = |c_{\eta nA}|^2 + |c_{\eta nB}|^2 \quad (112)$$

where we sum over all energy bands, valley, and spin. The  $\beta_{\eta n}$  term weights the contribution of

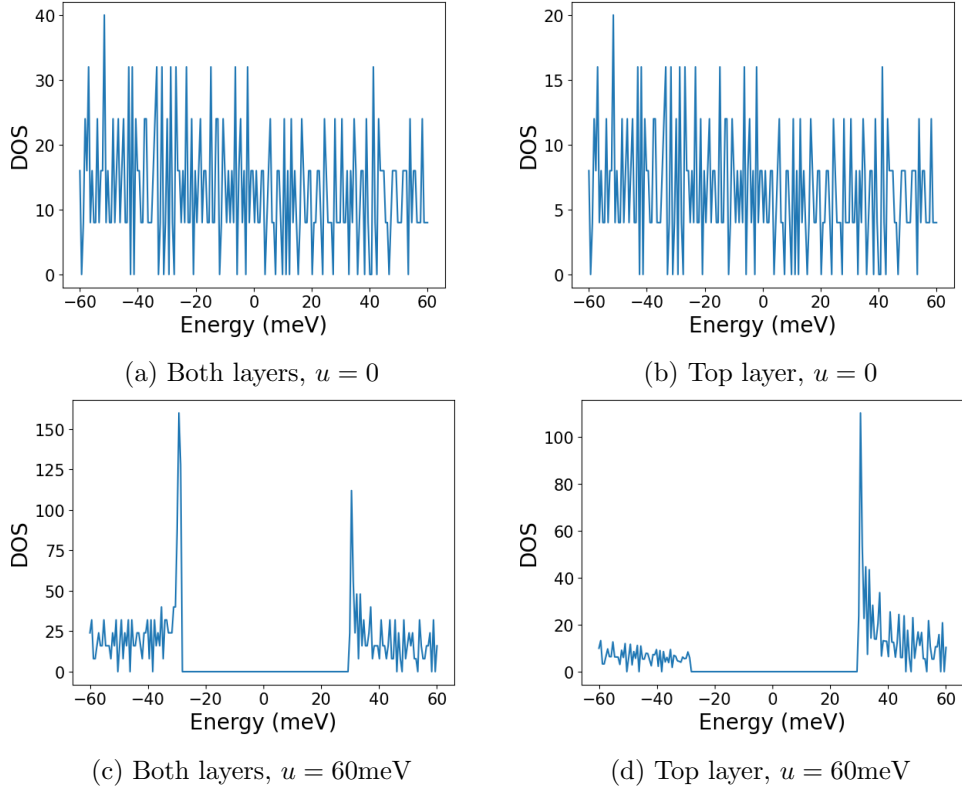


Figure 15: Numerical density of states (DOS) for bilayer graphene obtained using the tight-binding model at zero magnetic field  $B = 0$ . (a,b) We set  $u = 0$ , or neglect the intrinsic displacement field, and see that the DOS is split evenly between the top and bottom layers (note the vertical axes of the figures halves when restricting to the top layer). (c,d) We set  $u = 60\text{meV}$ , and see that when considering both layers, the DOS has two large spikes at the ends of the band gap, while when only considering the top layer, only the conduction band spike remains.

an energy band to the density of states by its presence on the top layer. To get the full density of states  $\text{DOS}(\varepsilon)$ , the  $\beta$  factor should be removed. The energy  $\varepsilon$  is measured with respect to the chemical potential  $\mu$ . Tuning the gate voltage  $V_g$  changes the filling factor and therefore changes the chemical potential. The amount the chemical potential changes depends on the number of states available at that level. If there are few states, then the chemical potential rises fast due to a small change in the gate voltage. We can express this relationship as  $d\mu/dV_g \propto 1/\text{DOS}(\mu)$ , or

$$V_g(\mu) \propto \int_0^\mu d\mu' \text{DOS}(\mu'). \quad (113)$$

which we can invert to obtain  $\mu(V_g)$ . We can then plot  $\text{DOS}_{AB}(\varepsilon - \mu(V_g))$  as a function of  $\varepsilon$  and  $V_g$  to simulate the density of states visible through STS. We require that  $V_g(\mu = 0) = 0$  since the sample is at charge neutrality when the gate voltage is  $V_g = 0$ .<sup>6</sup>

<sup>6</sup>When the intrinsic displacement  $D_0$  is introduced, an energy gap opens up at charge-neutrality splitting the valence and conduction bands. This energy gap is perfect in that the density of states completely vanishes within it. Therefore when tuning the gate voltage across this regime, there is a discrete jump in the chemical potential which we implement numerically by only keeping unique values of  $V_g(\mu)$ .

### 3.4 Fractional quantum Hall effect in bilayer graphene

Earlier we discussed the Halperin multi-component FQH state in the context of bilayer materials, and that it gives rise to interesting correlated electron interactions. In the case of bilayer graphene, there are a number of flavors we must take into account including spin, valley, and layer. The Landau level index also plays an important role in electron dynamics since the orbitals are heavily dependent on the energy level. For instance, we showed earlier that the  $n = 1$  Landau level of bilayer graphene consists of a combination of  $|0\rangle$  and  $|1\rangle$  states (localized on different sublattices). It turns out that the relative weight of the  $|0\rangle$  state increases with magnetic field  $B$ . On the other hand, the  $n = 0$  Landau level only consists of the  $|0\rangle$  state (localized on a single sublattice depending on valley). This rich interplay between flavors is responsible for novel FQH phases as compared to typical 2-dimensional electron gas semiconductor devices [2]. For instance, at  $n = 0$  only odd-denominator states which can be explained by a single-component composite fermion model have been observed. On the other hand, at  $n = 1$  the odd-denominator states are weaker except for  $\nu = 1/3$  and  $\nu = 2/3$  states. Even-denominator states, which we touched on briefly, have also been observed in the  $n = 1$  level but not  $n = 0$ .

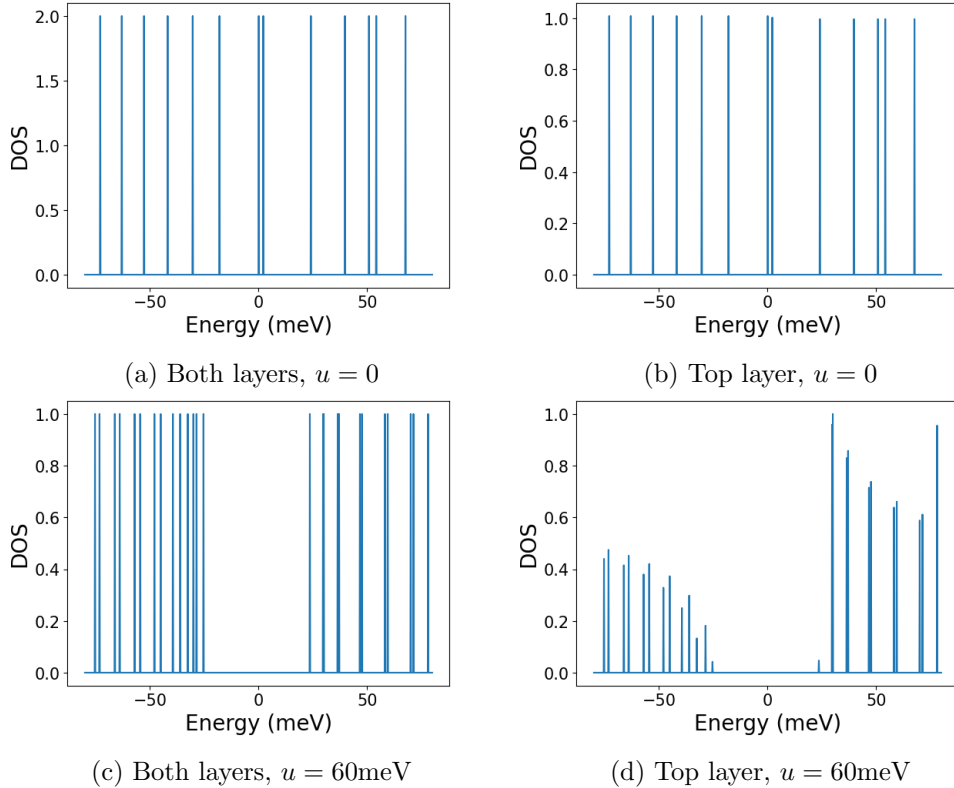


Figure 16: Numerical density of states (DOS) for bilayer graphene obtained using the tight-binding model at magnetic field  $B = 6\text{T}$ . (a,b) We set  $u = 0$  and see that the DOS is split evenly between the top and bottom layers. (c,d) We set  $u = 60\text{meV}$  and see that a band gap opens, similar to the  $B = 0$  case. The states also split forming close pairs of energy levels. When restricted to the top layer, the valence band spikes are more reduced compared to conduction band spikes.

The Halperin states can be generalized to multi-component composite fermion phases, a so-called expanded composite fermion model, where each attached flux tube (or interaction with Chern-Simons gauge field) has a flavor [2, 7]. In the single-component model, electrons of a particular

flavor only interact with flux tubes of the same flavor. However, we generalize this notion to include both intraflavor and interflavor flux attachment. As before, this model of attaching flux tubes forms composite fermions which experience a reduced magnetic field and have weaker interactions with each other. In the present case, the effective magnetic field is dependent on the electron density in all flavors and can be expressed as  $B_i^* = B - (an_i + bn_j)\Phi_0$  where  $i$  denotes the flavor index, and  $a, b$  are the number of intralayer and interlayer flux quantum attached per electron respectively. We now focus on the case of the layer flavor in bilayer graphene. If the layers have the same electron density  $n_i = n_j$ , then the composite fermion filling factor (of the Lambda levels) can be written as [2]

$$\nu_i^* = \nu_j^* = \frac{\nu}{1 - (a + b)\nu} \quad (114)$$

where  $\nu = \nu_1 = \nu_2$  is the electron filling factor of a single layer. This relation can be generalized for different electron densities  $n_i \neq n_j$

$$\nu_i^* = \frac{\nu_i}{1 - (a\nu_i + b\nu_j)}. \quad (115)$$

Note that there are a number of new properties which distinguish this model from the single-component composite fermion model. Once the electron densities are fixed, the composite fermions have a layer index but essentially do not interact with composite fermions of the opposite layer, and the problem almost becomes layer-independent. The composite fermions on each layer can experience different effective magnetic fields if the electron densities of the layers are not equal. Earlier in our discussion of composite fermions, we noted that an even number of flux tubes must be attached so that the resulting quasielectrons are fermions (to describe odd-denominator states). In the present case, only intralayer flux attachment must be an even number  $a$ , and interlayer flux attachment can take on any integer value ( $\leq a$ ) [2]. We denote  $a, b$  flux-attached composite fermions as  ${}_a^b\text{CF}$ . There have been numerous experimental measurements which suggest the existence of  ${}_2^2\text{CF}$ ,  ${}_1^2\text{CF}$  states in the same sample and applied field. It seems strange that with the layer separation fixed, there are composite fermion states of different interlayer flux attachment  $b = 1, 2$ . This has a number of important implications including that the layer separation does not solely determine the interlayer electron correlations. Indeed the interlayer correlations can be tuned via the electron density.

Of recent attention are the experimentally-observed even-denominator states (e.g.  $\nu = -1/2, 5/2$ ) [2]. Similar even-denominator states were also present in GaAs samples, but since it is enclosed by a semiconductor heterostructure, it is difficult to probe further. The scanning tunnelling spectroscopy technique we introduced earlier can probe the wave function of the even-denominator state by performing an LDOS measurement.

## 4 Conclusions

In this paper, we provided an overview of the integer and fractional quantum Hall effects and applied this theory to understand current developments in probing bilayer graphene using scanning tunnelling spectroscopy. We also developed a simple tight-binding model of bilayer graphene both with and without a magnetic field applied and computed the density of states. We see that the  $B = 0$  density of states at charge-neutrality match well with experimental data from the Yazdani Group. We are currently trying to understand the results of the  $B \neq 0$  density of states and will fine-tune parameters to hopefully better understand symmetry-breaking in bilayer graphene.

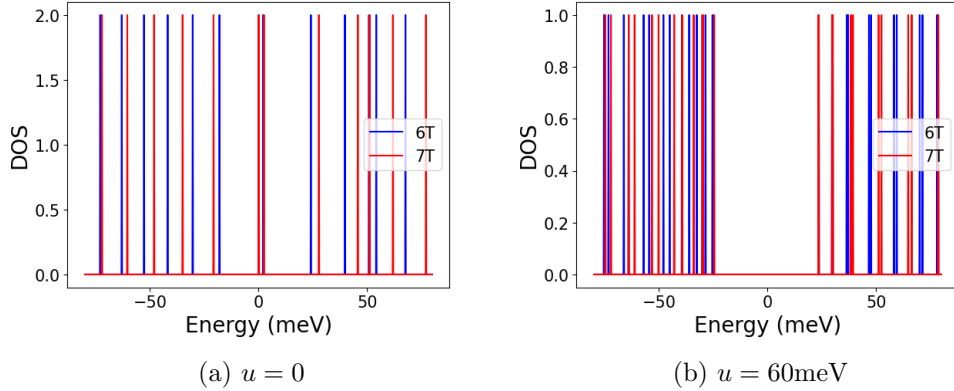


Figure 17: We vary the magnetic field  $B = 6, 7\text{T}$ , and see a shift in the energy levels for both the  $u = 0$  and  $u = 60\text{meV}$  cases. Take the difference in energy for each level and map them according to their orbital  $|n\rangle_{BG}$ . For the  $u = 60\text{meV}$ , the conduction band states roughly correspond to  $|n\rangle_{BG}$  for  $n = 0/1, 2, 3, 4, 3, 3$  respectively (from lower to higher energy) where the repeated levels correspond to different flavors.

An effort was made to perform Hartree-Fock computations, but they proved to complex for the duration of the term. Once the single-particle picture has been exhausted for understanding the data, returning to numerical simulations with interactions included could prove fruitful.

The code for the numerical simulations can be found at [https://github.com/amirsm02/mohammadi\\_yazdani\\_JPII](https://github.com/amirsm02/mohammadi_yazdani_JPII).

## Acknowledgements

I am especially grateful to Professor Ali Yazdani for spending so much of his time, both inside and outside of our scheduled meeting times, sharing his tremendous insight. It is an honor to work with someone on a field they are actively pioneering. I am grateful to Professor Duncan Haldane for discussing current research efforts in related fields after class and for being an endless reservoir of physics. I am also thankful to Professor Mansour Shayegan for his experimental insights into related fields. Thank you to all three of them for propelling my interest and passion in condensed matter, both theory and experiment. Thank you also to Yen-Chen Tsui, Yuwen Hu, Minhao He, and the Yazdani Lab for help with the measurement data and guiding the simulation results.

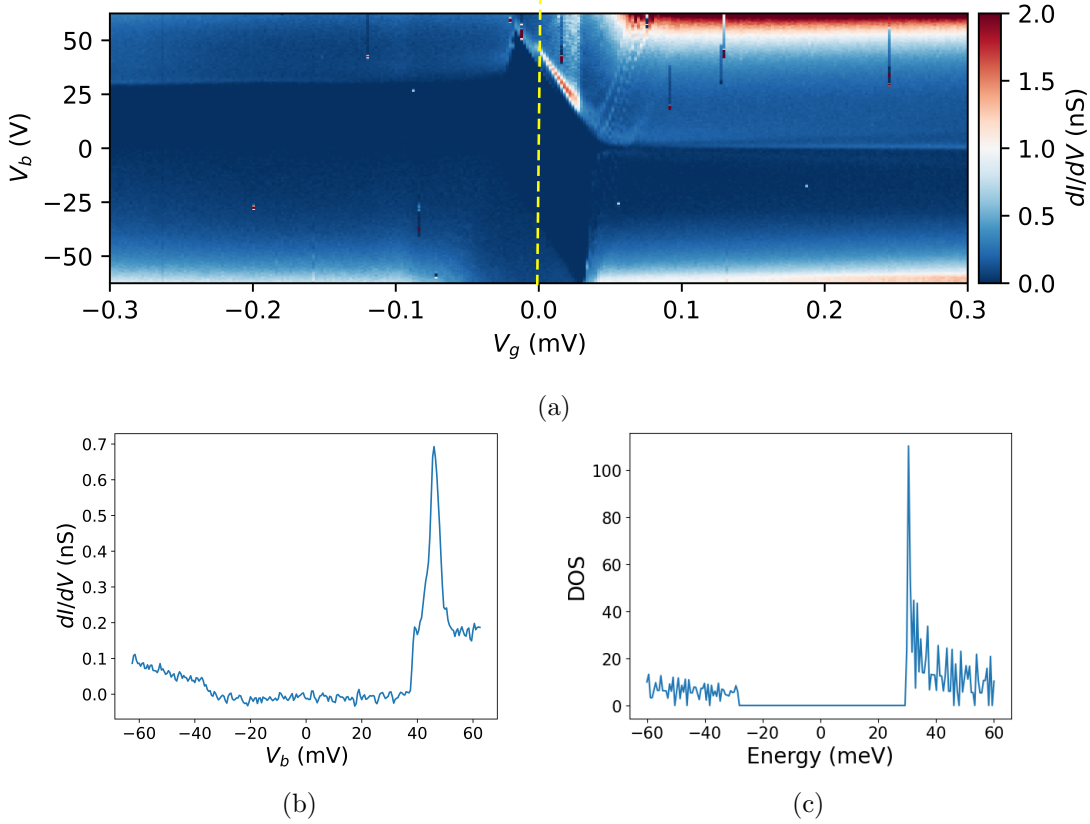


Figure 18: (a) Differential tunnelling conductance for  $B = 0$  measured as a function of gate voltage  $V_g$  and bias voltage  $V_b$  using STS [15]. (b,c) We select the  $V_g = 0$  cut at charge-neutrality (b) and note that it is similar to the  $u = 60$  meV DOS we numerically computed using the bilayer graphene tight-binding model (c). It may be that interactions play a significant role in the  $V_g = 0$  data that our model does not capture.

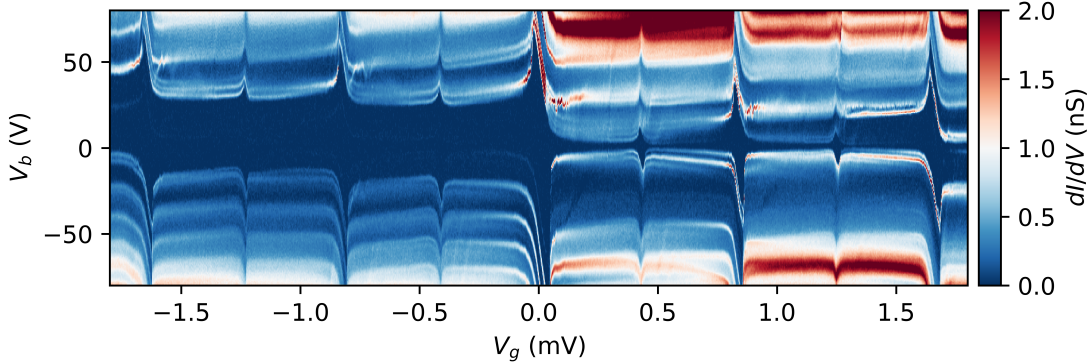


Figure 19: Differential tunnelling conductance for  $B = 6$  T showing bilayer graphene Landau levels. Note that some of the layers are less visible than others since they are presumably located on the bottom layer. There are also splittings of many of the Landau levels which is currently not fully explained by any model. There are also numerous integer quantum Hall phases opening gaps in the energy levels [15].

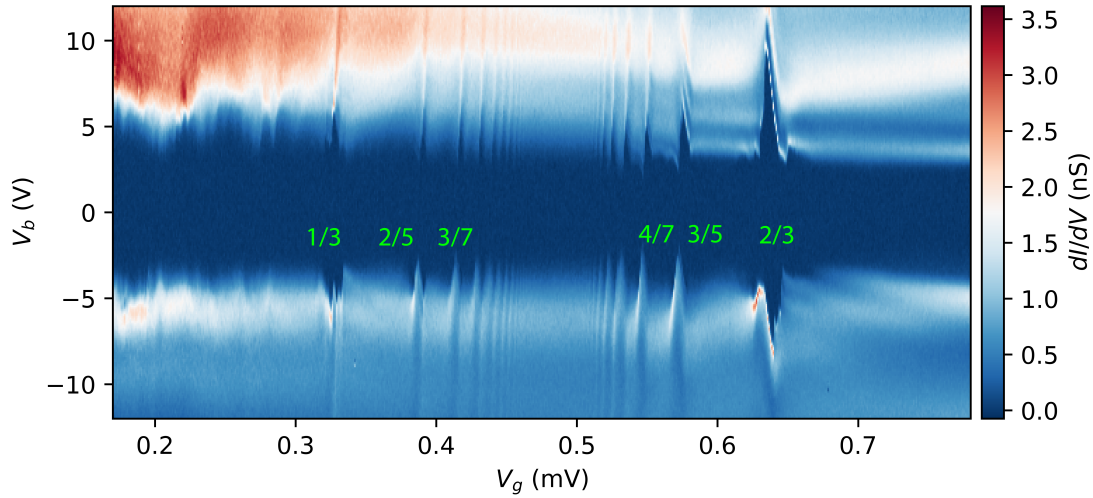


Figure 20: A magnified view of the previous STS figure shows energy gaps opening at the Jain sequence filling factors, indicating FQH phases. Some of the filling factors are indicated [15].

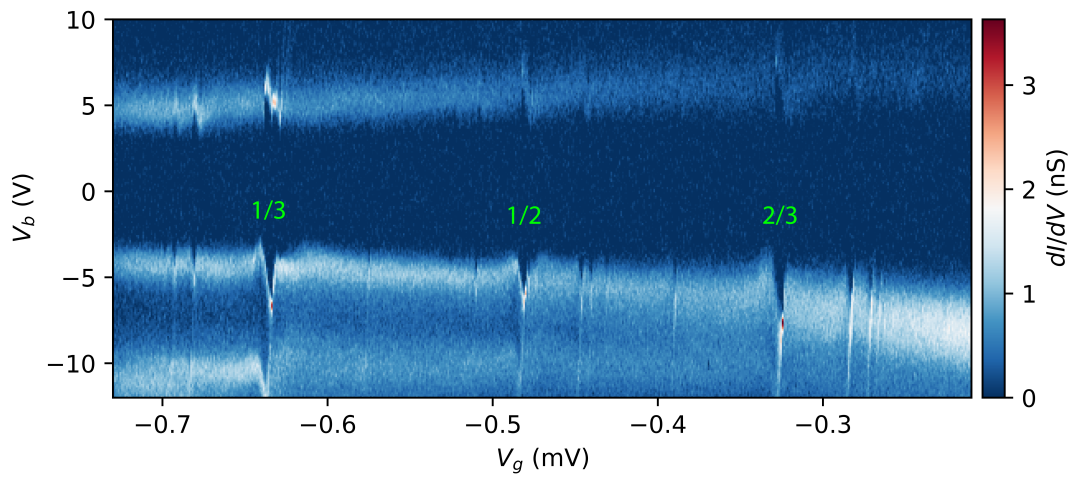


Figure 21: STS measurement of the  $n = 2$  bilayer graphene Landau level  $1 \leq \nu \leq 2$  showing a  $\nu = 3/2$  ( $\equiv 1/2$ ) even denominator state [15].

## References

- [1] Yang Cheng et al. “Emerging properties of two-dimensional twisted bilayer materials\*”. In: *Chinese Physics B* 28.10 (2019), p. 107304. DOI: 10.1088/1674-1056/ab3e46.
- [2] Cory Dean et al. “Fractional Quantum Hall Effects in Graphene”. In: *Fractional Quantum Hall Effects* (2020), pp. 317–375. DOI: 10.1142/9789811217494\_0007.
- [3] Z. Y. Ezawa. *Quantum Hall Effects: Field theoretical approach and related topics*. World Scientific, 2000.
- [4] Steven M. Girvin and Kun Yang. *Modern Condensed Matter Physics*. Cambridge University press, 2019.
- [5] Maria Vittoria Gurrieri. “Twisted bilayer graphene: Effective model, topological states and relevant symmetries”. In: *University of Bologna* (2020).
- [6] B. M. Hunt et al. “Direct measurement of discrete valley and orbital quantum numbers in bilayer graphene”. In: *Nature Communications* 8.1 (2017). DOI: 10.1038/s41467-017-00824-w.
- [7] Jainendra Jain. *Composite fermions*. Cambridge University Press, 2012.
- [8] K. v. Klitzing, G. Dorda, and M. Pepper. “New method for high-accuracy determination of the fine-structure constant based on quantized hall resistance”. In: *Physical Review Letters* 45.6 (1980), pp. 494–497. DOI: 10.1103/physrevlett.45.494.
- [9] R. B. Laughlin. “Anomalous Quantum Hall Effect: An Incompressible Quantum Fluid with Fractionally Charged Excitations”. In: *Quantum Hall Effect: A Perspective* (1983), pp. 231–234. DOI: 10.1007/978-94-010-9709-3\_26.
- [10] Biao Lian. “PHY525: Introducion to condensed matter physics”. In: *Department of Physics, Princeton University* ().
- [11] Ronaldo Rodrigues Pela. *Physical Properties of Graphene*. URL: <http://exciting.wikidot.com/oxygen-physical-properties-of-graphene>.
- [12] H.L. Stormer. “Two-dimensional electron correlation in high magnetic fields”. In: *Physica B: Condensed Matter* 177.1-4 (1992), pp. 401–408. DOI: 10.1016/0921-4526(92)90138-i.
- [13] J. Tersoff and N.D. Lang. “Theory of scanning tunneling microscopy”. In: *Scanning Tunneling Microscopy* (1993), pp. 1–29. DOI: 10.1016/b978-0-12-674050-9.50007-4.
- [14] D. C. Tsui, H. L. Stormer, and A. C. Gossard. “Two-dimensional Magnetotransport in the extreme quantum limit”. In: *Physical Review Letters* 48.22 (1982), pp. 1559–1562. DOI: 10.1103/physrevlett.48.1559.
- [15] Yen-Chen Tsui et al. “Scanning tunneling microscopy study of robust fractional quantum Hall states in Bernal-stacked bilayer graphene”. In: *APS March Meeting 2023* ().